Accepted Manuscript

A novel class of thiosemicarbazones show multi-functional activity for the treatment of Alzheimer's disease

Duraippandi Palanimuthu, Rachal Poon, Sumit Sahni, Rukhsana Anjum, David Hibbs, Hsuan-Yu Lin, Paul V. Bernhardt, Danuta S. Kalinowski, Des R. Richardson

PII: S0223-5234(17)30624-4

DOI: 10.1016/j.ejmech.2017.08.021

Reference: EJMECH 9665

To appear in: *European Journal of Medicinal Chemistry*

Received Date: 2 June 2017

Revised Date: 7 July 2017

Accepted Date: 7 August 2017

Please cite this article as: D. Palanimuthu, R. Poon, S. Sahni, R. Anjum, D. Hibbs, H.-Y. Lin, P.V. Bernhardt, D.S. Kalinowski, D.R. Richardson, A novel class of thiosemicarbazones show multi-functional activity for the treatment of Alzheimer's disease, *European Journal of Medicinal Chemistry* (2017), doi: 10.1016/j.ejmech.2017.08.021.

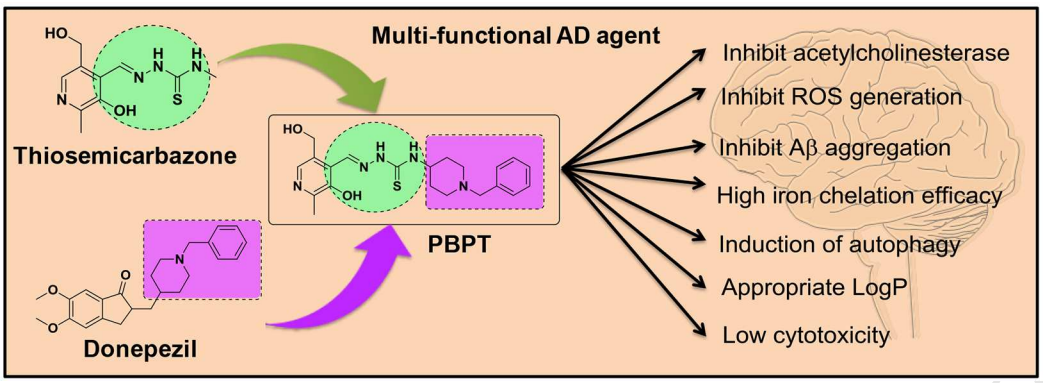

A Novel Class of Thiosemicarbazones Show Multi-Functional Activity for the Treatment of Alzheimer's Disease

Duraippandi Palanimuthu[a], Rachal Poon[a], Sumit Sahni[a], Rukhsana Anjum[a], David Hibbs[b], Hsuan-Yu Lin[b], Paul V. Bernhardt[c], Danuta S. Kalinowski[a*] and Des R. Richardson[a*]

[a]*Molecular Pharmacology and Pathology Program, Department of Pathology and Bosch Institute The University of Sydney, Sydney, New South Wales, 2006, Australia,*

[b]*Faculty of Pharmacy, The University of Sydney, Sydney, New South Wales, 2006, Australia.*

[c]*School of Chemistry and Molecular Biosciences, University of Queensland, Brisbane, 4072, Australia.*

*__Corresponding authors:__ Dr. Des R. Richardson and Dr. Danuta S. Kalinowski; Molecular Pharmacology and Pathology Program, Discipline of Pathology, Blackburn Building (D06), The University of Sydney, Sydney, New South Wales 2006, Australia. Tel.: + 61 2 9036-6548; Fax: +61 2 9351-3429; Email: d.richardson@med.usyd.edu.au; danuta.kalinowski@sydney.edu.au

ABBREVIATIONS

AD, Alzheimer's disease; Aβ, amyloid-β; ACh, acetylcholine; AChE, acetylcholinesterase; BBB, blood-brain barrier; PBT2, 5,7-dichloro-2-dimethylaminomethyl-8-hydroxyquinoline; ROS, reactive oxygen species; BPT, 4-(1-benzylpiperidin-4-yl)thiosemicarbazone; DFO, desferrioxamine; Dp44mT, di-2-pyridylketone 4,4-dimethyl-3-thiosemicarbazone; NBPT, 2-hydroxy-1-naphthaldehyde 4-(1-benzylpiperidin-4-yl)thiosemicarbazone; 2,3-OH-BBPT, 2,3-dihydroxybenzaldehyde 4-(1-benzylpiperidin-4-yl)thiosemicarbazone; 2,3,4-OH-BBPT, 2,3,4-trihydroxybenzaldehyde 4-(1-benzylpiperidin-4-yl)thiosemicarbazone; 8-OH-QBPT, 8-hydroxy-2-quinolinecarboxaldehyde 4-(1-benzylpiperidin-4-yl)thiosemicarbazone; PBPT, pyridoxal 4-(1-benzylpiperidin-4-yl)thiosemicarbazone; PCBPT, 2-pyridinecarboxaldehyde 4-(1-benzylpiperidin-4-yl)thiosemicarbazone; QBPT, 2-quinolinecarboxaldehyde 4-(1-benzylpiperidin-4-yl)thiosemicarbazone; SBPT, salicylaldehyde 4-(1-benzylpiperidin-4-yl)thiosemicarbazone; PBS, phosphate-buffered saline; DTNB, 5,5′-dithiobis(2-nitrobenzoic acid); DTPA, diethylenetriaminepentaacetic acid; EDTA, ethylenediaminetetraacetic acid; HEPES, 2-[4-(2-hydroxyethyl)piperazin-1-yl]ethanesulfonic acid; MTT, 3-(4,5-dimethylthiazol-2-yl)-2,5-diphenyltetrazolium bromide; Tf, transferrin.

Abstract

Over 44 million people live with Alzheimer's disease (AD) worldwide. Currently, only symptomatic treatments are available for AD and no cure exists. Considering the lack of effective treatments for AD due to its multi-factorial pathology, development of novel multi-target-directed drugs are desirable. Herein, we report the development of a novel series of thiosemicarbazones derived from 1-benzylpiperidine, a pharmacophore within the acetylcholinesterase inhibitor, Donepezil. These thiosemicarbazones were designed to target five major AD hallmarks, including: low acetylcholine levels, dysfunctional autophagy, metal dys-homeostasis, protein aggregation and oxidative stress. Of these thiosemicarbazones, pyridoxal 4-(*N*-(1-benzylpiperidin-4-yl)thiosemicarbazone (PBPT) emerged as the lead compound. This agent demonstrated the most promising multi-functional activity by exhibiting very low anti-proliferative activity, substantial iron chelation efficacy, inhibition of copper-mediated amyloid-β aggregation, inhibition of oxidative stress, moderate acetylcholinesterase inhibitory activity and autophagic induction. These diverse properties highlight the potential of the lead ligand, PBPT, as a promising multi-functional agent for AD treatment.

Keywords: Alzheimer's disease, acetylcholinesterase, thiosemicarbazone, iron chelator, oxidative stress, autophagy.

1. Introduction

Alzheimer's disease (AD) is the most common form of dementia in which neurons, particularly in the hippocampus and entorhinal cortex region, undergo multiple and complex biochemical changes that result in progressive memory loss and cognitive decline [1-3]. The expected increase in the rate of dementia cases is predicted to be 3- to 4-fold higher in developing nations than in developed nations [4].

Extensive examination of neuro-pathological and neuro-physiological studies revealed that five major hallmarks concomitantly contribute to AD progression, including: **(1)** decreased acetylcholine (ACh) levels [5]; **(2)** dys-homeostasis of metal metabolism [6]; **(3)** amyloid-β (Aβ) and tau aggregation, resulting in the generation of senile plaques and neurofibrillary tangles, respectively [7]; **(4)** generation of oxidative stress [8]; and **(5)** the dysregulation of autophagy [9].

ACh is a neurotransmitter released by cholinergic neurons that are responsible for cognition [10,11], and unfortunately, these cholinergic cells degenerate in AD patients [12]. As a result, ACh levels decline markedly in the central nervous system of AD patients [13]. Several acetylcholinesterase (AChE) inhibitors, including the FDA approved drugs, Donepezil (**Fig. 1**) [14], Rivastigmine and Galantamine, have been shown to enhance cholinergic transmission by inhibiting the degradation of ACh into choline [15,16]. Nevertheless, these agents do not alter the course of AD.

Dys-homeostasis of bioavailable transition metal ions, such as iron (Fe), copper (Cu), and zinc (Zn), are considered to be another hallmark of AD [6,17]. In fact, these metal ions were found to accumulate at 3- to 7-fold higher levels in AD patients than in healthy individuals and modulate several key intracellular events that relate to AD pathology [18]. The accumulation of Fe, Cu and Zn are thought to facilitate the self-aggregation of Aβ *via* metal-peptide chelation to form senile

plaques, which are deposited outside of neurons [19]. Moreover, Fe in its Fe(III) state is thought to contribute to the aggregation of hyper-phosphorylated tau protein to form intracellular neurofibrillary tangles [20]. The inappropriate accumulation of redox-active Fe and Cu also causes oxidative damage to neurons *via* the generation of deleterious reactive oxygen species (ROS) through Haber-Weiss and Fenton-type reactions [8]. The resultant oxidative damage is consequently implicated in Aβ peptide aggregation [8].

Chelation therapy has been proposed as potentially useful for the treatment of AD [6,21,22], with the clioquinol-based chelator, 5,7-dichloro-2-dimethylaminomethyl-8-hydroxyquinoline (PBT2), mediating an improvement in cognition *via* inhibition of metal-induced Aβ aggregation in pre-clinical mice models and a human Phase I clinical trial [23]. Subsequent phase II clinical trials demonstrated that PBT2 was well tolerated in patients with mild AD, but larger trials are necessary to demonstrate efficacy in terms of cognitive improvement [24].

Autophagy is a major degradation mechanism in the cell that plays a central role in neuroprotection by facilitating the removal of aggregated proteins [25]. However, impaired autophagic clearance in AD has been suggested to lead to incomplete lysosomal/autolysosomal digestion and the accumulation of partially digested peptides, such as Aβ and tau, which aggregate to form senile plaques and neurofibrillary tangles, respectively [26,27].

In view of the complex multifactorial etiology of AD described above, an effective treatment for AD is likely to require an agent with multiple mechanisms of action that can simultaneously target the major hallmarks of the disease. This therapeutic strategy is in contrast to current therapeutics for this disease that target only one major facet of AD pathology and provide symptomatic relief without treating the underlying disease processes [28]. To target the multiple pathologies of AD, multi-target directed ligands that fuse active pharmacophores from various ligands represents a

promising drug design strategy [28-36]. Notably, several multi-target directed ligands that incorporate the benzylpiperidine pharmacophore from Donepezil to inhibit AChE have been examined as novel therapeutics for AD [29,37-39]. Moreover, multi-target directed ligands that utilize metal chelators have also shown some promising therapeutic potential [36,37,40]. Considering this, we have developed a series of novel compounds that contain the benzylpiperidine pharmacophore from Donepezil and the metal-chelating thiosemicarbazone moiety (**Fig. 1**). This design strategy enables: **(1)** chelation of redox-active metals (to prevent ROS generation and the production of protein aggregates); **(2)** inhibition of AChE activity (to increase ACh levels); and **(3)** the induction of autophagy (to remove toxic protein aggregates). Moreover, the unique group of thiosemicarbazones designed in this investigation demonstrated generally low cytotoxicity, which is another key property for AD treatment.

2. Results and Discussion

2.1 Design Strategy

Thiosemicarbazones demonstrate potent metal chelation activity both *in vitro* and *in vivo* [41,42]. In our laboratory, we have utilized this molecular scaffold to develop various biologically active ligands [43,44]. These agents are lipophilic and highly bioavailable with appropriate pharmacokinetics and potently bind metal ions, such as Fe and Cu [45], that play a major role in the pathogenesis of AD [46]. Recently Gomes *et al.* identified that 8-hydroxyquinoline-based thiosemicarbazones also inhibit Cu-induced Aβ aggregation by sequestering Cu, and thus, these agents have anti-oxidant potential [47]. All these properties inspired us to implement a lipophilic thiosemicarbazone scaffold in our drug design strategy for AD treatment.

Donepezil is an AChE inhibitor clinically used to treat AD that consists of the benzylpiperidine and indanone moieties. Recent crystallographic studies have revealed that the benzylpiperidine fragment interacts with the catalytic active site of AChE to inhibit the enzyme, whereas the indanone fragment interacts with the peripheral anionic site of AChE through aromatic stacking interactions [38,48,49]. Therefore, we incorporated the benzylpiperidine moiety at the terminal N4 atom of the thiosemicarbazone backbone to mediate AChE inhibition (**Fig. 1**). Moreover, we chose various aldehydes with different donor atom capacities (*i.e.*, N,N,S or O,N,S), which plays an important role in the redox chemistry of their metal complexes and aromatic character in order to generate a variety of thiosemicarbazones to assess their therapeutic potential.

2.2 Chemistry

The reagent, 4-(1-benzylpiperidin-4-yl)thiosemicarbazide, was prepared from 4-amino-1-benzylpiperidine as shown in **Scheme 1** using a standard procedure [50]. The resulting thiosemicarbazide was then further reacted with appropriate aroyl aldehydes by the Schiff base condensation route to generate 4-(1-benzylpiperidin-4-yl)thiosemicarbazone (BPT) derivatives.

These agents were thoroughly characterized by ^{1}H and ^{13}C NMR (**Supplementary Material Figs. S1-S8**), electrospray ionization mass spectrometry (ESI-MS; **Figs. S9-S16**), and in some cases, by X-ray crystallography and the purity assessed by elemental analysis. The resulting ligands were sparingly soluble in water and ethanol, but were completely soluble in polar aprotic solvents, such as DMF and DMSO. Indeed, pharmacologically relevant concentrations were readily prepared from DMSO stock solutions of 20 mM to generate stable working solutions of ≤ 100 μM in cell culture media (DMSO final concentration: ≤ 0.5% v/v).

We also synthesized the resultant 1:1 (Cu(II)/ligand) copper complexes and 1:2 (Fe(III)/ligand) iron complexes (see **Supplementary Material** for synthesis and characterization). The Cu complexes were prepared by refluxing equimolar amounts of the thiosemicarbazone and cupric chloride in ethanol, whereas the iron complexes were prepared by reaction of an aqueous ethanol solution of the thiosemicarbazone with ferric perchlorate at a 2:1 mole ratio. This was done to satisfy the octahedral coordination of iron with the tridentate thiosemicarbazone ligands. All these complexes were characterized by standard techniques, including electrospray ionization-mass spectroscopy (ESI-MS), elemental analysis, and in one case, by X-ray crystallography.

2.3 X-ray Diffraction

The structures of the ligands and resultant metal complexes are important to decipher in order to completely understand their biological activity. The molecular structures of the ligands, [HSBPT][OAc] and PCBPT, were determined using single crystal X-ray crystallography (**Fig. 2A, B;** crystallographic data is available in the **Supplementary Material: Table S1**). The crystal structure of [HSBPT][OAc] finds the piperidine N-atom (N4) protonated (**Fig. 2A**) and strongly H-bonded to the acetate anion (N4−H…O3 1.73 Å, 173.84°). In this case, acetic acid from the synthesis has carried through to the final product. The acetate anion is also H-bonded to the phenol OH group from an adjacent molecule (O1−H…O2 1.75 Å, 166.6°). The phenol OH is *anti* to the

imine N-atom (N1). The atoms, N1 and S1, are also in an *anti*-disposition (**Fig. 2A**), so the ligand must rearrange in the presence of a metal ion in order to bind as a tridentate chelator.

The crystal structure of PCBPT (**Fig. 2B;** crystallographic data is available in **Table S1**) reveals a similar ligand conformation with the potential donor atom pairs N1/N2 and N2/S1 also in an *anti*-configuration. In this case, the piperidine N-atom is not protonated and the only H-bonding contact of note in the structure of PCBPT involves an intermolecular interaction between the thiosemicarbazone NH and the pyridyl ring (N3−H…N1 2.17 Å, 163.4°). The chelating moieties of both [HSBPT][OAc] and PCBPT (extending from the phenol/pyridyl ring to the thiosemicarbazone N4-atom) are essentially flat and all dihedral angles in this region are within 6° of planarity.

The crystal structure of the Cu complex, [Cu(SBPT)Cl_2], was also determined (**Fig. 2C;** crystallographic data can be found in **Table S1**). The thiosemicarbazone ligand coordinates in a zwitterionic form with deprotonation of the phenolic OH (O1) and protonation of the piperidine N-atom (N4). The coordination geometry is formally axially elongated square pyramidal (**Fig. 2C**), with one equatorially bound chlorido ligand (Cu−Cl1 2.2613(8) Å) and one very weakly bound chlorido ligand in the axial coordination site (Cu…Cl2 2.9045(8) Å). The thiosemicarbazone coordinates in its thioamide tautomeric form, and thus, the thiocarbonyl bond (C8−S1 1.712(3) Å) has essentially double bond character and is not significantly different from that found in the structure of [HSBPT][OAc] above (1.693(1)) Å). Other chlorido Cu(II) complexes of salicylaldehyde thiosemicarbazones also are found exclusively in the thioamide form (N(H)−C=S−Cu) [51,52]. However, there is a large variation in the Cu-S coordinate bond length within these analogues (2.226(2)−2.2785(8) Å) with the bond in [Cu(SBPT)Cl_2] being the longest of the series. Interestingly, other chlorido thiosemicarbazone Cu complexes are genuinely square planar [53]. Hence, it appears that the negative charge of the weakly coordinated axial chlorido ligand in [Cu(SBPT)Cl_2] is responsible for elongating the Cu-S bond in this structure (**Fig. 2C**).

2.4 Electrochemistry and EPR Spectroscopy of Copper and Iron Complexes

Several studies, including those performed in our laboratories, have shown that the biological activity of thiosemicarbazones is often associated with their ability to mediate Fenton chemistry upon complexation with intracellular Fe and Cu [43,54,55]. Therefore, we examined the electrochemical behavior of the prepared copper and iron complexes in buffered DMF: H_2O (7:3). This solvent combination was particularly used to ensure solubility and to enable comparisons to our previous studies that have examined a broad range of thiosemicarbazone complexes using this solvent mixture [56,57]. EPR spectroscopy was also used to probe the nature of the paramagnetic Cu(II) or Fe(III) metal ions.

Copper Complexes: The EPR spectra of the copper complexes of PBPT, SBPT and NBPT, suggested formation of mixtures of 1:1 $Cu^{II}L$ complexes with different coordination modes in a DMF:H_2O (7:3) solution (**Fig. S17**). It appears that bidentate N,S (peaks marked with a *) and tridentate O,N,S (peaks marked with a $^{\#}$) are possible coordination modes, where the tridentate species is preferred over the bidentate species for these complexes. However, no evidence of CuL_2 species formation was observed (**Fig. S17**). The cyclic voltammetric data (**Fig. S18**) further indicate that these complexes exhibit an irreversible Cu(II/I) couple (reduction to Cu(I) followed by rapid partial dissociation of one ligand with re-oxidation at a higher potential).

The EPR data of the copper complexes of PCBPT, QBPT and 8-OH-QBPT indicate the formation of mixtures of 1:1 CuL complexes again with bi- (N,S) and tridentate (N,N,S) coordination (**Fig. S17**). Notably, the copper QBPT complex is dominantly present as a bidentate coordinated complex. This is possibly due to steric effects repelling the quinoline ring, while the Cu complexes of PCBPT and 8-OH-QBPT could be a 50:50 mixture. This latter suggestion is supported by the cyclic voltammetry, where the higher potential Cu(II/I) wave for the copper QBPT complex (bidentate coordinated complex) is separate from the overlapping lower potential wave of tridentate

copper PCBPT complex and its higher potential bidentate complex wave (**Fig. S18**). The copper complexes of 8-OH-QBPT showed two reduction waves.

Interestingly, the Cu complexes of 2,3-OH-BBPT and 2,3,4-OH-BBPT again form mixtures of 1:1 CuL complexes, where the tridentate species is more favored for Cu 2,3-OH-BBPT and bidentate for Cu 2,3,4-OH-BBPT (**Fig. S17**). The 2,3-OH-BBPT Cu complex exhibited a markedly lower redox potential compared to the other Cu complexes (**Fig. S18**). None of the Cu(II) complexes are able to undergo reversible reduction to Cu(I).

Iron Complexes: The 1:2 Fe:L complexes exhibited a variety of properties across this series of ligands. The Fe complexes of PBPT, SBPT, NBPT, PCBPT, QBPT and 2,3-OH-BBPT all showed EPR spectra consistent with low spin Fe(III) complexes in axial or rhombic ligand fields (**Fig. S19**). The four O,N,S bis-ligand Fe(III) complexes (PBPT, SBPT, NBPT and 2,3-OH-BBPT) gave similar axial EPR spectra (g_z, g_y = 2.134, g_x = 1.920), while the corresponding N,N,S Fe(III) complexes of PCBPT and QBPT showed rhombic spectra, but with significantly different g values; g_z = 2.134, g_y = 2.094, g_x = 1.960 and g_z = 2.150, g_y = 2.076, g_x = 1.970, respectively. The greater g-aniosotropy in the quinoline containing Fe(III)-QBPT complex suggests a structure that is more distorted from octahedral symmetry than in the pyridyl analogue, PCBPT. The EPR spectrum of the Fe complex of 8-OH-QBPT demonstrated that it is a high spin Fe(III) complex, while the Fe complex of 2,3,4-OH-BBPT was EPR silent. This finding strongly suggested that the latter is a Fe(II) complex.

Cyclic voltammetry of the Fe complexes showed a similar diversity of behavior (**Fig. S20**). The O,N,S-coordinated Fe complexes of PBPT, SBPT, NBPT, 8-OH-QBPT and 2,3-OH-QBPT are essentially the same exhibiting a low potential cathodic peak (~ −400 mV *vs.* NHE) and an anodic peak at approximately 0 mV. This is indicative of a rapid partial dissociation of the complex upon reduction to Fe(II), which is then re-oxidized at a higher potential. The low potential at which these

complexes are reduced strongly suggests that they will not be redox active under biological conditions. In contrast, the Fe complexes of the N,N,S ligands, PCBPT and QBPT, exhibit totally reversible Fe(III/II) couples at approximately +130 mV *vs*. the normal hydrogen electrode (NHE). These latter data are very similar to characterized pyridyl thiosemicarbazone complexes we have reported previously [54]. The Fe complex of 2,3,4-OH-BBPT does not exhibit any metal-centered redox responses in the potential range investigated.

2.5 The Anti-Proliferative Activity of the BPT Analogues and their Metal Complexes Using SK-N-MC Neuroepithelioma Cells

Having demonstrated that the BPT analogues can form copper and iron complexes, studies then assessed their anti-proliferative activity using SK-N-MC neuroepithelioma cells after a 72 h incubation (**Table 1**). This cell-type was used as it has been implemented as a neural cell model in studies assessing agents for the treatment of AD [58,59]. The well-characterized metal chelators, di-2-pyridylketone 4,4-dimethyl-3-thiosemicarbazone (Dp44mT), a chelator with potent anti-proliferative activity [43,44], and desferrioxamine (DFO), a clinically used chelator for iron overload disease [60], were used as controls as their anti-proliferative efficacy against SK-N-MC cells is well described [44,60]. We also assessed the cytotoxicity of the clinically used AD drug, Donepezil, which was implemented as a scaffold for the design of BPT analogues (**Fig. 1**). In these studies, DFO and Dp44mT displayed IC_{50} values of 16.81 μM and 0.013 μM, respectively (**Table 1**), which is in good agreement with our previous studies examining these agents [44,61]. However, Donepezil, showed no appreciable anti-proliferative activity with an IC_{50} value of >100 μM (**Table 1**).

Importantly, all the novel BPT series of agents showed poor anti-proliferative activity and significantly ($p < 0.001$) decreased anti-proliferative efficacy relative to Dp44mT (**Table 1**). Notably, PBPT demonstrated an IC_{50} value that was >100 μM and was the least cytotoxic of all the

novel agents examined (**Table 1**). Similarly, SBPT, 8-OH-QBPT and 2,3,4-OH-BBPT showed low anti-proliferative activity (*i.e.*, IC_{50}: 34.41 μM, 36.14 μM and 79.14 μM, respectively) and were significantly ($p < 0.001$) less effective than DFO (**Table 1**). Both 2,3-OH-BBPT and QBPT showed IC_{50} values (IC_{50}: 16.85 μM and 17.71 μM, respectively) that were comparable ($p > 0.05$) to DFO (**Table 1**). The ligands, NBPT and particularly PCBPT, demonstrated the greatest anti-proliferative activity of the BPT series (IC_{50}: 8.86 μM and 4.23 μM, respectively), with IC_{50} values that were significantly ($p < 0.001$) less than DFO (**Table 1**).

The greater anti-proliferative efficacy of PCBPT relative to the other BPT agents could be due to the ability of this N,N,S ligand to form redox active Fe complexes after binding intracellular Fe (as described above; see *Electrochemistry and EPR Spectroscopy of Copper and Iron Complexes*). Indeed, our laboratory has shown previously that such N,N,S ligands demonstrate high anti-proliferative activity [43,54]. In summary, these data demonstrate the low anti-proliferative activity of the BPT series in SK-N-MC cells, which supports their utility as agents for AD treatment.

Since the BPT analogues were designed to form metal complexes with endogenous copper and iron, we also examined the anti-proliferative efficacy of their 1:1 Cu: ligand and 1:2 Fe: ligand complexes towards SK-N-MC cells (**Table 1**). The anti-proliferative activity of the copper and iron complexes of the controls, DFO, Dp44mT and Donepezil, were also assessed. The Cu complex of DFO showed a significant ($p < 0.001$) increase in anti-proliferative activity relative to the free ligand, as observed previously [62]. Although the Cu complex of Dp44mT showed similar anti-proliferative activity to its free ligand, Donepezil in the presence of Cu demonstrated increased anti-proliferative activity relative to Donepezil alone (**Table 1**). As shown previously [62], the Fe complexes of DFO and Dp44mT showed significantly ($p < 0.001$) decreased anti-proliferative activity compared to their respective ligands (**Table 1**). The anti-proliferative efficacy of Donepezil in the presence of iron was similar to that observed for Donepezil alone (>100 μM; **Table 1**).

It is apparent that all the novel Cu complexes of the BPT analogues displayed significantly ($p < 0.001$) higher anti-proliferative activity than the corresponding ligands (**Table 1**). Interestingly, the Fe complexes of all novel chelators, except PCBPT and QBPT, exhibited significantly ($p < 0.001-0.05$) lower anti-proliferative efficacy compared to their respective ligands (**Table 1**). These findings suggest that the Fe complexes of the BPT ligands, apart from those derived from PCBPT and QBPT, are not biologically reactive (*e.g.*, in terms of ROS generation). This was in concordance with the low potential at which these Fe complexes are reduced (see above: *Electrochemistry and EPR Spectroscopy of Copper and Iron Complexes*). In contrast, the Fe complexes of PCBPT and QBPT exhibited significantly ($p < 0.001$) potentiated cytotoxicity compared to the corresponding ligands. Again, this observation was in good agreement with the electrochemistry of their Fe complexes, which was reversible, and within a range previously demonstrated to lead to redox activity [43,54].

In summary, the BPT series have generally low anti-proliferative efficacy. While Fe complexation resulted in generally attenuated cytotoxicity, Cu complexation led to potentiated cytotoxic effects relative to the free ligand. Although Cu complexation increased their anti-proliferative efficacy of the BPT ligands, it is notable that the activity of the novel Cu complexes was markedly less than that of Dp44mT or its Cu complex (**Table 1**). Collectively, amongst the BPT series of analogues, PBPT and its Fe or Cu complex demonstrated the poorest anti-proliferative efficacy, which is a desirable characteristic for the long-term treatment of AD.

2.6 The Effect of the BPT Analogues on ^{59}Fe Release from Prelabeled Cells

Accumulation of Fe is a common feature of AD brains [8,63], which leads to oxidative stress through the generation of ROS and aggregation of both Aβ and tau [6]. We examined the Fe chelation efficacy of the BPT analogues to evaluate their ability to bind intracellular Fe and release it from SK-N-MC neuroepithelioma cells (**Fig. 3A**). These results were compared to three controls,

namely: **(1)** Dp44mT, a well characterized thiosemicarbazone with high Fe mobilization efficacy [43]; **(2)** DFO, a clinically used chelator implemented for the treatment of Fe overload disease [64] and also AD [65] that has poor BBB permeability, and thus, low efficacy [66]; and **(3)** Donepezil, an AChE inhibitor used for AD treatment [48], which is not a known chelator, but was used as a control, as the current BPT series contains a pharmacophore-derived from this inhibitor (**Fig. 1**).

In these experiments, SK-N-MC cells were prelabeled with the physiological ^{59}Fe donor, diferric transferrin ($^{59}Fe_2$-Tf), washed and then reincubated with control medium, or medium containing the agents (25 μM) using standard methods [56,61,67]. Levels of ^{59}Fe in the cells and ^{59}Fe released into the overlying medium were then assessed [56,61,67]. As previously observed [56], the incubation of prelabeled SK-N-MC cells with control medium alone resulted in minimal cellular ^{59}Fe release (6% of total cellular ^{59}Fe; **Fig. 3A**). The positive control, Dp44mT, significantly ($p < 0.001$) increased ^{59}Fe mobilization to 49% of total cellular ^{59}Fe (**Fig. 3A**). In contrast, DFO showed limited ability to induce ^{59}Fe release from cells, leading to the mobilization of 15% of cellular ^{59}Fe (**Fig. 3A**), which was significantly ($p < 0.001$) higher than control medium, but was significantly ($p < 0.001$) lower than Dp44mT (**Fig. 3A**). Donepezil did not show any significant ($p > 0.05$) effect on ^{59}Fe release compared to control medium (**Fig. 3A**), confirming that Donepezil does not act as an iron chelator due to the lack of appropriate ligating moieties (**Fig. 1**).

All novel BPT analogues showed the ability to significantly ($p < 0.001$) increase cellular ^{59}Fe mobilization compared to the control, but were significantly ($p < 0.001$) less effective than Dp44mT (**Fig. 3A**). Notably, PBPT, SBPT and 2,3-OH-BBPT were the most effective of the BPT analogues and significantly ($p < 0.001$) increased ^{59}Fe release (*i.e.*, 31%, 28% and 29%, respectively) relative to DFO (**Fig. 3A**). Additionally, NBPT, PCBPT, 8-OH-QBPT and 2,3,4-OH-BBPT showed comparable ^{59}Fe mobilization efficacy (*i.e.*, 16%, 18%, 17% and 14%, respectively) to that of DFO. Finally, QBPT showed the poorest ability to mediate cellular ^{59}Fe release (10% of cellular ^{59}Fe) of

this series and was significantly ($p < 0.01$) less active than DFO (**Fig. 3A**). No strong correlation was observed between the ability of the BPT series to mediate cellular ^{59}Fe release and their log P_{calc} values (R^2 = 0.3274) or IC_{50} values (R^2 = 0.0264). Collectively, amongst this series of analogues, PBPT, SBPT and 2,3-OH-BBPT demonstrated the greatest efficacy at mobilizing cellular ^{59}Fe.

2.7 The Effect of the BPT Series on Inhibiting ^{59}Fe Uptake from ^{59}Fe-Transferrin

Considering the ability of the BPT analogues to induce cellular ^{59}Fe release, experiments then examined the activity of these agents to inhibit iron uptake from $^{59}Fe_2$-Tf by SK-N-MC cells (**Fig. 3B**). In these studies, the chelators (25 µM) were incubated with cells in the presence of $^{59}Fe_2$-Tf, which physiologically donates iron to cells *via* endocytosis [68]. The ability of the chelators to inhibit the internalization of ^{59}Fe into cells was examined using standard methodology [61,67]. As utilized in the iron mobilization studies above, Dp44mT, DFO and Donepezil (25 µM) were implemented as relevant controls (**Fig. 3B**).

As previously observed [43], Dp44mT could markedly and significantly ($p < 0.001$) inhibit cellular ^{59}Fe uptake to 5% of the control (**Fig. 3B**). On the other hand, DFO was significantly ($p < 0.001$) less effective than Dp44mT, but still significantly ($p < 0.001$) decreased cellular ^{59}Fe uptake to 85% of the control (**Fig. 3B**). Donepezil showed little activity (96% of the control) at reducing ^{59}Fe uptake due to the lack of effective chelation moieties and was significantly (p<0.001-0.01) less effective than Dp44mT or DFO (**Fig. 3B**).

Overall, the BPT series demonstrated varying ability to inhibit cellular ^{59}Fe uptake (**Fig. 3B**). All of the BPT analogues were significantly ($p < 0.001$-0.01) more effective than control media alone, but were significantly ($p < 0.001$) less effective than Dp44mT at inhibiting cellular ^{59}Fe uptake (**Fig. 3B**). Notably, PBPT was the most effective agent of the BPT series and decreased cellular ^{59}Fe

uptake to 41% of the control (**Fig. 3B**). The analogues, PBPT (41%), SBPT (57%), NBPT (68%), PCBPT (63%) and 2,3-OH-BBPT (63%), were significantly ($p < 0.001$) more effective than DFO (**Fig. 3B**). The least effective analogues at reducing ^{59}Fe uptake were QBPT, 8-OH-QBPT and 2,3,4-OH-BBPT, which inhibited ^{59}Fe uptake to 91%, 78% and 93% of the control, respectively (**Fig. 3B**). While QBPT and 8-OH-QBPT showed comparable efficacy to DFO, 2,3,4-OH-BBPT showed significantly ($p < 0.05$) lower efficacy at inhibiting ^{59}Fe uptake relative to DFO (**Fig. 3B**).

As demonstrated with ^{59}Fe mobilization experiments, no strong correlation was observed between their ability to inhibit ^{59}Fe uptake and either their Log P_{calc} values ($R^2 = 0.2064$) or IC_{50} values ($R^2 = 0.3094$). In conclusion, PBPT demonstrated the most promising ability of the BPT analogues at inhibiting cellular ^{59}Fe internalization from $^{59}Fe_2$-Tf.

2.8 The Effect of the Iron Complexes of the BPT Series on Ascorbate Oxidation

An important property of chelators for the treatment of Fe-loading conditions is that they should bind and remove excess Fe from tissues and also form redox-inactive Fe complexes. This is critical in diseases, such as AD, where iron accumulation occurs within plaques and has been reported to play a detrimental role in inducing oxidative stress [8].

To examine their redox properties, the Fe(III) complexes of the BPT series of ligands were assessed in terms of their ability to catalyze ascorbate oxidation *via* Fe-mediated Fenton chemistry [56,69]. In these studies, ascorbate was used as a substrate because of its abundance in neurons and its strong anti-oxidant potential to protect these cells from oxidative stress [70-72]. For comparison, the well-known, redox-active Fe(III) complexes of EDTA and Dp44mT were included as positive controls [54,56,73]. On the other hand, the redox inactive Fe(III) complex of DFO was used as a negative control since it inhibits oxidative stress [54,56,73]. Moreover, we also assessed the ability of Donepezil to mediate ascorbate oxidation in the presence of Fe(III) (**Fig. 1**). The ascorbate

oxidation activity of the Fe complexes of QBPT and 2,3,4-OH-BBPT could not be determined (N.D.) due to their low solubility under the conditions used in this assay.

In accordance with our previously published results [54,56,73], the EDTA- and Dp44mT-Fe(III) complexes markedly and significantly ($p < 0.001$) accelerated ascorbate oxidation to 436% and 285% of the control, respectively (**Fig. 4A**). In contrast, the redox-inactive Fe(III)-DFO complex significantly ($p < 0.001$) reduced ascorbate oxidation, decreasing it to 29% of the control, confirming its anti-oxidative activity (**Fig. 4A**). Additionally, in the presence of Fe(III), Donepezil showed comparable levels of ascorbate oxidation relative to control (**Fig. 4A**).

Generally, all but one of the Fe(III) complexes of the BPT analogues did not accelerate ascorbate oxidation (**Fig. 4A**) compared to the control. In fact, the Fe(III) complexes of these agents significantly ($p < 0.001$) decreased ascorbate oxidation when compared to the iron complexes of EDTA or Dp44mT (**Fig. 4A**). However, all iron complexes of the BPT series showed significantly ($p < 0.001$) increased levels of ascorbate oxidation relative to DFO (**Fig. 4A**). The Fe(III) complexes of PBPT, NBPT, 8-OH-QBPT and 2,3-OH-BBPT significantly ($p < 0.001$) reduced ascorbate oxidation to 61%, 52%, 69% and 79% of the control, respectively (**Fig. 4A**), suggesting their anti-oxidant activity. In contrast, the Fe(III) complex of PCBPT mediated significantly ($p < 0.001$) increased levels of ascorbate oxidation to 212% of the control (**Fig. 4A**), suggesting its pro-oxidative activity. This observation is in agreement with the reversible cyclic voltammogram observed for this Fe complex. The Fe(III) complex of SBPT demonstrated a slightly, but significantly ($p < 0.01$), lower level of ascorbate oxidation (93%) relative to the control (**Fig. 4A**). Collectively, the Fe(III) complexes of PBPT, NBPT, 8-OH-QBPT and 2,3-OH-BBPT inhibited ascorbate oxidation relative to the control. These observations suggest that these ligands have the potential to alleviate the Fe-mediated oxidative stress observed in AD.

2.9 The Ability of the BPT Series to Inhibit Hydrogen Peroxide-Mediated Cytotoxicity

To further examine the ability of the BPT series of agents to protect cells against oxidative stress that is a hallmark of AD [8], experiments were conducted to examine their efficacy in terms of protecting SK-N-MC cells from hydrogen peroxide (H_2O_2)-mediated cytotoxicity (**Fig. 4B**). In these experiments, cells were pre-incubated for 2 h/37°C with either: serum-free control medium, the BPT analogues, or the control agents, DFO or Donepezil, at a concentration of 10 μM [74]. The medium was then removed and the cells incubated with serum-free medium alone, or serum-free medium containing H_2O_2 (150 μM) for 24 h/37°C. Cellular proliferation was then assessed using the MTT assay. In these studies, Dp44mT was not used as a control due to its potent cytotoxicity under the conditions implemented for these experiments.

The incubation of control cells with medium containing H_2O_2 led to a significant ($p < 0.001$) decrease in cellular proliferation to 56% of the control (**Fig. 4B**). Importantly, over the short incubation utilized (24 h), the control agents, DFO and Donepezil alone, did not exhibit any significant ($p > 0.05$) anti-proliferative activity relative to the control (**Fig. 4B**). Additionally, these agents also protected cells from H_2O_2-mediated cytotoxicity, with DFO and Donepezil significantly ($p < 0.001$) increasing cellular proliferation to 89% and 74%, respectively, relative to control cells incubated with H_2O_2 (**Fig. 4B**).

Pre-incubation of cells with PBPT or SBPT alone did not demonstrate any significant ($p > 0.05$) effect on proliferation relative to control cells (**Fig. 4B**). In contrast, NBPT, PCBPT, QBPT, 8-OH-QBPT, 2,3-OH-BBPT, or 2,3,4-OH-BBPT alone mediated a significant ($p < 0.001$-0.05) decrease in cellular proliferation (58-94%) relative to control cells (**Fig. 4B**). All of the BPT analogues, except NBPT, could alleviate the H_2O_2-mediated inhibition of proliferation and significantly ($p < 0.001$-0.01) increased proliferation to 66-87% of the control relative to control cells incubated with H_2O_2

alone (**Fig. 4B**). Notably, the inability of NBPT to alleviate the H_2O_2-mediated inhibition of proliferation is likely due to the potential cytotoxicity of this ligand itself. (**Fig. 4B**).

Collectively, these studies demonstrated that all BPT analogues (except NBPT) could alleviate H_2O_2-mediated anti-proliferative activity. Both PBPT and SBPT were able to alleviate H_2O_2-mediated inhibition of proliferation without inducing cytotoxic effects on their own, suggesting their potential to prevent oxidative stress in AD.

2.10 Acetylcholinesterase (AChE) Inhibition by the BPT Series

As another integral component of its complex pathology, low acetylcholine levels are implicated to play a role in the cognitive decline in AD [75]. The inhibition of AChE has been demonstrated to increase ACh levels in the brain and alleviate cognitive deficits, with several AChE inhibitors already commercially available in the clinics (*e.g.*, Donepezil) [48,76,77]. To induce AChE inhibition, the benzylpiperidine scaffold of Donepezil was chosen as a key fragment to be combined with the thiosemicarbazone moiety as the benzylpiperidine moiety of Donepezil strongly interacts with the active site of AChE [49]. Thus, the BPT series were examined for their *in vitro* inhibitory activity against AChE and their potencies were compared to the well-known AChE inhibitors, Donepezil and Tacrine [78]. The inhibition of AChE by the agents was expressed as IC_{50} values and presented in **Fig. 5**.

As expected, the positive controls, Donepezil and Tacrine, showed potent inhibition of AChE with IC_{50} values in the sub-micromolar range, namely 0.067 and 0.11 μM, respectively (**Fig. 5**). In contrast, all novel BPT analogues demonstrated IC_{50} values in the micromolar range (1.02 - 22.61 μM), which were significantly ($p < 0.001$-0.01) increased relative to that of Donepezil and Tacrine. Among the BPT analogues, NBPT and 2,3-OH-BBPT exhibited the greatest AChE inhibition, with IC_{50} values of 1.23 and 1.02 μM, respectively (**Fig. 5**).

When comparing the IC_{50} values of the mono- (*i.e.*, SBPT), di- (*i.e.*, 2,3-OH-BBPT), and tri-hydroxy (*i.e.*, 2,3,4-OH-BBPT) benzaldehyde analogues, it was found that the di-hydroxy analogue, 2,3-OH-BBPT, showed the most potent AChE inhibitory activity with an IC_{50} value of 1.02 μM (**Fig. 5**). However, either the removal (SBPT) or addition (2,3,4-OH-BBPT) of a single hydroxyl group resulted in a significant ($p < 0.001$) decrease in AChE inhibitory activity relative to 2,3-OH-BBPT by 4.5- or 22.2-fold, respectively (**Fig. 5**). Interestingly, the pyridoxal analogue, PBPT, that contains one hydroxyl group bonded directly to the pyridoxal ring, showed an IC_{50} value (4.93 μM) that was similar to SBPT, despite the presence of other substituents on the ring. The pyridine analogue (PCBPT), devoid of a hydroxyl group, showed lower activity compared to SBPT (**Fig. 5**). Together, these results suggest that 2,3-OH-BBPT bearing two hydroxyl groups showed better AChE inhibition.

The fusion of an additional aromatic ring to either pyridine (to form QBPT and 8-OH-QBPT), or salicylaldehyde (to form NBPT) resulted in increased AChE inhibitory activity by at least 3-fold relative to their single aromatic ring counterparts (*i.e.*, PCBPT and SBPT, respectively; **Fig. 5**). This observation suggests that the additional aromatic moiety enhances the hydrophobic interactions with AChE. Hence, these structure-activity relationships provide impetus for future synthetic approaches.

In summary, all compounds, except 2,3,4-OH-BBPT, showed the potential to act as moderate AChE inhibitors.

2.11 Molecular Docking Studies

To understand the mode of interaction between the BPT analogues and AChE, we performed molecular docking studies of the most active AChE inhibitor, 2,3-OH-BBPT (IC_{50} = 1.02 μM), and the lead compound, PBPT (IC_{50} = 4.93 μM), in comparison to Donepezil in the active site of the

human AChE enzyme (PDB ID: 4EY7). This was performed implementing the molecular mechanics generalized born approach using the molecular volume integration and surface area model (MM-GBSA) *via* the GLIDE extra precision (GLIDE-XP) program [79]. The most probable ligand-protein interaction at the active site was estimated that resulted in a negative GLIDE docking score and binding free energies (MMGBSA-dG-Bind).

As expected, the positive control, Donepezil, resulted the highest docking score (-19.63 kcal/mol) with good binding affinity (-88.30 kcal/mol), suggesting its strong interaction with AChE. The most active BPT analogue, 2,3-OH-BBPT, also showed a strong interaction with AChE as evident from the docking score (-17.12) and binding free energy (-88.29 kcal/mol). The lead compound, PBPT, also strongly interacted with AChE, but showed a poorer docking score (-15.12) and binding energy (-83.59 kcal/mol) than 2,3-OH-BBPT. The docking diagrams (**Fig. 6**) further suggest that the BPT analogues bind to AChE utilizing a similar binding mode to that of Donepezil (**Fig. 6A**). For instance, the piperidine NH^+ of both 2,3-OH-BBPT and PBPT interact with TRP86 and TYR337 through pi-cation interactions (**Fig. 6B,C**) in a similar manner to Donepezil (**Fig. 6A**). Additionally, the phenyl ring of 2,3-OH-BBPT and PBPT interact with TRP86 *via* π-π interactions (**Fig. 6B,C**), as observed for Donepezil (**Fig. 6A**). Collectively, these docking studies support the AChE inhibition data (**Fig. 5**) and highlight the pivotal role of the benzylpiperidine moiety in the interaction of the BPT analogues with AChE.

2.12 The Effect of the BPT Series on Inhibiting Copper-Mediated $A\beta_{1-40}$ Aggregation

It is well known that elevated levels of trace metal ions, including Cu, Zn and Fe, can be detected in Aβ plaque deposits [80]. Furthermore, Cu(II) and Zn(II) facilitate the self-aggregation of the $A\beta_{1-40}$ and $A\beta_{1-42}$ peptides [81], of which the $A\beta_{1-40}$ isoform is abundant in cerebrospinal fluid [82]. Therefore, we assessed the ability of the BPT analogues to inhibit the Cu(II)-mediated aggregation of $A\beta_{1-40}$ using an established turbidity assay [47,83,84]. These studies were performed by

incubating equimolar concentrations of $A\beta_{1-40}$ (25 µM) and Cu(II) (25 µM) in the presence or absence of the BPT ligands (25 µM) in HEPES buffer (pH 6.6) followed by scattering measurements at 405 nm [47]. The slightly acidic pH of the HEPES buffer was utilized because Cu(II) facilitates robust Aβ aggregation at this pH [84], and also because acidosis is a common characteristic of AD brains [85]. Several controls were also implemented, including: **(1)** the chelator, diethylenetriamine pentaacetic acid (DTPA), which is a known inhibitor of Cu(II)-induced Aβ aggregation [47]; **(2)** the well-characterized copper chelating thiosemicarbazone, Dp44mT [43,86]; and **(3)** the clinically used AChE inhibitors, Donepezil and Tacrine.

As shown in **Fig. 7**, the co-incubation of Cu(II) with $A\beta_{1-40}$ significantly ($p < 0.001$) enhanced Aβ aggregation relative to $A\beta_{1-40}$ alone. Upon addition of the positive control, DTPA, a significant ($p < 0.001$) reduction in Cu(II)-mediated $A\beta_{1-40}$ aggregation was observed, which is likely to be due to its ability to chelate Cu(II), as demonstrated previously [47]. Similarly, Dp44mT, markedly and significantly ($p < 0.001$) inhibited Cu(II)-mediated $A\beta_{1-40}$ aggregation. In contrast, the AChE inhibitors, Donepezil and Tacrine, did not demonstrate any significant ($p > 0.05$) effect on Cu(II)-mediated $A\beta_{1-40}$ aggregation, which is likely due to their inability to chelate Cu(II).

Of all of the novel BPT analogues, PCBPT, 8-OH-QBPT and especially 2,3-OH-BBPT, exhibited the greatest ability to inhibit Cu(II)-mediated $A\beta_{1-40}$ aggregation, followed by 2,3,4-OH-BBPT, PBPT, SBPT and QBPT. All of these aforementioned ligands significantly ($p < 0.001$-0.05) inhibited Cu(II)-mediated $A\beta_{1-40}$ aggregation. In fact, the ability of 8-OH-QBPT and 2,3-OH-BBPT to inhibit Cu(II)-mediated $A\beta_{1-40}$ aggregation was comparable to that observed with DTPA. The ability of NBPT to inhibit the Cu(II)-mediated aggregation of $A\beta_{1-40}$ could not be determined (N.D.) due to its low solubility under the conditions of this assay.

Overall, these studies demonstrated (in order of decreasing efficacy) that 2,3-OH-BBPT, 8-OH-QBPT, PCBPT, 2,3,4-OH-BBPT, SBPT, QBPT and PBPT displayed the ability to inhibit Cu(II)-mediated $A\beta_{1-40}$ aggregation, demonstrating their therapeutic value for AD treatment. Similar results to those reported here with $A\beta_{1-40}$ were also obtained upon examining the ability of the novel BPT analogues to inhibit Cu(II)-mediated $A\beta_{1-42}$ aggregation (**Fig. S21**).

2.13 The Effect of the BPT Analogues on the Expression of the Autophagic Marker, p62

Studies were initiated to examine the effect of the BPT agents on autophagy, as it is a catabolic pathway involved in the clearance of damaged cellular proteins and organelles [87]. Dysfunctional autophagy has been linked with AD pathology and the accumulation of aggregated proteins, such as Aβ and tau [26,27]. Thus, it was imperative to study the effect of our novel agents on this pathway. Initially, the effect of our compounds on the protein, p62, was examined as a useful marker of autophagy [88]. This protein is involved in the delivery of damaged cargo to autophagosomes and its levels are known to be inversely related to autophagic flux in the cell, *i.e.*, low p62 is observed if there is high autophagic activity and *vice versa* [88].

In these studies, SK-N-MC cells were incubated with the BPT analogues (25 µM) for 24 h/37°C. The effect of our novel agents was directly compared to Dp44mT (25 µM), which has been previously shown to activate the autophagic pathway [89,90]. The levels of p62 were shown to be significantly ($p < 0.001$) decreased after incubation with Dp44mT compared to control cells, suggesting increased autophagic activity (**Fig. 8A-H**). This result is in contrast to previous studies in which Dp44mT was observed to increase p62 levels *via* increased autophagic initiation and decreased autophagic completion [90]. The difference between our results and those previously observed [90] can be explained by the different cell-types implemented (*e.g.*, SK-N-MC neuroepithelioma cells *cf.* to MCF7, MDA-MB-231 and T47D breast cancer cell-types) and different incubation conditions utilized (*e.g.*, concentration of 25 µM *cf.* to 0.01-5 µM).

Incubation with NBPT (**Fig. 8A, B)** or SBPT (**Fig. 8E, F**) led to a slight, but significant ($p < 0.01$-0.05) increase in p62 levels compared to control cells. However, there was no significant ($p > 0.05$) change in p62 levels after incubation with PBPT, 2,3-OH-BBPT, PCBPT, QBPT, 8-OH-QBPT, or 2,3,4-OH-BBPT compared to control cells (**Fig. 8A-H**). The lack of change observed in p62 levels after incubation with the latter BPT analogues may be due to an increase in overall autophagic flux, *i.e.*, both increased formation and degradation of autophagosomes. Thus, the next set of studies assessed the effect of these agents on the autophagic initiation and degradation pathway to assess the autophagic flux and dissect the mechanism involved.

2.14 The Effect of the BPT Analogues on Autophagic Initiation

As autophagy is a dynamic process (**Fig. 9Ai**), it was crucial to determine the ability of the BPT analogues to affect autophagic flux. To assess this, the late-stage autophagy inhibitor, Bafilomycin A1 (Baf A1), was implemented using standard procedures [88]. In these experiments, SK-N-MC cells were pre-incubated for 30 min with the late-stage autophagy inhibitor, Baf A1 (100 nM), followed by co-incubation of Baf A1 and Dp44mT (a known inducer of autophagy; 25 µM) [89,90] or the novel BPT analogues (25 µM) for 24 h/37°C (**Fig. 9B-I**). Incubation of cells with Baf A1 is known to inhibit the late-stage autophagic degradation process *via* a dual mechanism, namely: **(1)** prevention of lysosomal acidification; and **(2)** inhibition of autophagosome-lysosome fusion (**Fig. 9Aii**) [88].

The lysates obtained from SK-N-MC cells treated with our ligands with or without Baf A1 were assessed for levels of LC3-II, which is a classical marker for autophagosomes [88]. Importantly, LC3-II is present on the autophagosome throughout its lifetime and is a reliable indicator of the quantity of autophagosomes present in the cell (**Fig. 9Ai**) [88].

Autophagy is a catabolic process that is constantly turning over cellular constituents and the synthesis and degradation of LC3-II is in constant flux under basal conditions (**Fig. 9Ai**). In the presence of Baf A1, the degradation of the autophagosome, and thus, LC3-II, is inhibited under basal conditions and results in an accumulation of this protein (**Fig. 9Aii**) [88]. Upon the addition of an autophagic inducer (*e.g.*, Dp44mT) [89,90], the synthesis of autophagosomes, and thus, LC3-II, is enhanced in comparison to basal levels and leads to a further increase in LC3-II accumulation when autophagosome turnover is inhibited by Baf A1 (**Fig. 9Aiii**). In contrast, an agent that inhibits autophagosomal degradation would not mediate a further increase in LC3-II levels upon the addition of Baf A1 relative to the basal LC3-II levels in the presence of Baf A1. Hence, *via* the utilization of Baf A1, the effect of agents on autophagosome turnover can be established, that is, if the agent affects autophagic initiation or autophagosomal degradation [87,88].

As shown previously [90], there was a marked and significant ($p < 0.001$) increase in LC3-II (18 kDa) levels after incubation of cells with Baf A1 alone (*i.e.*, Baf A1-treated control cells) compared to the control cells (**Fig. 9B-I**). The levels of LC3-II observed after incubation of control cells with Baf A1 represents basal autophagic initiation and the basal number of autophagosomes generated under these conditions (**see Fig. 9Aii**) [88]. Notably, as shown in previous studies [89,90], upon incubation of cells with Baf A1 and the positive control, Dp44mT, there was a significant ($p < 0.001$) increase in LC3-II levels compared to cells incubated with Baf A1 alone (**Fig. 9B-I**). This observation demonstrates that Dp44mT can initiate the autophagy pathway in SK-N-MC cells to increase autophagosome number (**see Fig. 9Aiii**), as demonstrated previously in other cell-types [89,90].

In cells incubated with PBPT, PCBPT, 8-OH-QBPT, or 2,3,4-OH-BBPT along with Baf A1, a significant ($p < 0.01$-0.05) increase in LC3-II levels was observed compared to control cells incubated with Baf A1 alone (**Fig. 9B-E,H,I**). Again, this demonstrates that these agents can

stimulate the autophagic initiation pathway in SK-N-MC cells. In contrast, there was no significant ($p > 0.05$) increase of LC3-II levels after incubation of cells with NBPT, 2,3-OH-BBPT, SBPT or QBPT along with Baf A1, when compared to control cells incubated with Baf A1 alone (**Fig. 9B-G**).

Moreover, upon examination of the effect of these agents alone (in the absence of Baf A1) on LC3-II levels, there was a slight, but significant ($p < 0.001$-0.05) increase only upon incubation with NBPT, 2,3-OH-BBPT or 8-OH-QBPT relative to the control (**Fig. 9B-E,H,I**). However, as shown above through BafA1 inhibitor studies, NBPT and 2,3-OH-BBPT were unable to induce autophagic initiation (**Fig. 9B-E**). Hence, the observed increase in LC3-II mediated by NBPT and 2,3-OH-BBPT can be attributed to inhibition of the autophagosomal degradation pathway by these BPT ligands.

Taken together, these studies demonstrate that PBPT, PCBPT, 8-OH-QBPT and 2,3,4-OH-BBPT increase autophagic initiation, while NBPT, 2,3-OH-BBPT, and SBPT inhibit the autophagic degradation pathway in SK-N-MC cells. In contrast, QBPT did not inhibit nor induce autophagic initiation. The ability of some of these agents (*e.g.*, PBPT) to increase autophagic initiation may be useful in order to clear protein aggregates (*e.g.*, Aβ), which is a major problem in AD [27].

2.15 Evaluation of Physicochemical Parameters to Cross the Blood-Brain Barrier (BBB)

Considering the promising multiple activities of the BPT analogues against key AD targets reported above and to further assess their potential drug-like properties, we subjected all of the novel BPT analogues to "Lipinski's Rule of Five" that analyzes crucial physicochemical properties to predict their druglikeness (see **Table 2**) [91]. All of the novel BPT ligands obeyed Lipinski's Rule of Five, along with the well-known AChE inhibitors, Tacrine and Donepezil (**Table 2**).

To predict the BBB permeation of these compounds that is crucial for AD treatment, other physicochemical properties, such as cLogP, topological polar surface area (TPSA) and LogBB (the logarithm of brain to blood concentration ratio) were considered (**Table 2**). These indices were examined as they are considered as reliable and major descriptors, which dictate the ability of compounds to cross the BBB and enhance their concentrations in the cerebrospinal fluid [92,93]. Based on studies examining the properties of marketed CNS drugs, it was considered that successful CNS agents will have a TPSA value less than 90 Å [93], a cLogP value between 2−5 [93], and a LogBB value greater than −1 [92].

As shown in **Table 2**, Tacrine, Donepezil and all BPT analogues, except 2,3,4-OH-BBPT, have cLogP, TPSA and LogBB values within or close to the desirable range for all parameters. Interestingly, the lead agent, PBPT, has appropriate cLogP (2.69) and LogBB (-0.82) values, and a TPSA value (92.48) close to the desired range. Hence, PBPT may cross the BBB and act as a potential CNS drug. For 2,3,4-OH-BBPT, the cLogP (2.82) and LogBB (-0.92) values are within the allowed range, but the TPSA value (100.35) increased dramatically relative to the other BPT analogues due to the presence of tri-hydroxyl groups. In summary, most of the novel BPT series demonstrate appropriate physicochemical characteristics that suggest their druglikeness and facilitates their BBB permeation to act as orally-available drugs for the CNS.

3. Conclusions

AD is a multi-factorial disease characterized by multiple pathological hallmarks that include low acetylcholine levels, dys-regulation of metal metabolism, oxidative stress, impaired autophagy and aggregation of Aβ [5-9]. In the current studies, we successfully demonstrated that multi-functional agents can be designed to synergistically target several major hallmarks of AD. In our design strategy, the amalgamation of several pharmacophores from different agents was utilized, resulting in a novel series of multi-functional drugs. In fact, these pharmacophores included: ***(1)*** the 1-benzylpiperidine fragment taken from the structure of the clinically used AChE inhibitor, Donepezil; and ***(2)*** the thiosemicarbazone moiety was used to target the chelation of redox-active metals to alleviate oxidative stress.

Using this strategy, we generated eight novel BPT analogues by condensing 1-benzylpiperidine thiosemicarbazide with various aldehydes. These BPT analogues and particularly PBPT generally demonstrated: ***(1)*** low anti-proliferative activity that was comparable to the well-tolerated clinically used iron chelator, DFO [60]; ***(2)*** better iron chelation efficacy than DFO; ***(3)*** the inhibition of Fe(III)-mediated ascorbate oxidation; ***(4)*** moderate AChE inhibitory activity; ***(5)*** the inhibition of Cu(II)-mediated aggregation of $A\beta_{1-40}$; and ***(6)*** increased autophagic initiation.

Of all of the BPT analogues examined, PBPT showed the most promising multi-functional activity and emerged as a lead agent for the treatment of AD. This compound was found to have limited anti-proliferative activity at concentrations of ≤ 100 μM in SK-N-MC cells and was able to mobilize cellular ^{59}Fe, as well as inhibit ^{59}Fe uptake from $^{59}Fe_2$-Tf. These data indicate that PBPT has favorable iron chelation properties that could facilitate the removal of excessive iron from extracellular Aβ plaques. Furthermore, PBPT significantly inhibited Fe(III)-mediated ascorbate oxidation and also alleviated the cytotoxic effects of hydrogen peroxide, suggesting its ability to act in a protective manner to prevent ROS generation. Additionally, this compound showed moderate

AChE inhibition and was also able to decrease the copper-mediated aggregation of $A\beta_{1-40}$. PBPT also demonstrated the ability to induce autophagy flux, suggesting this ligand may be able to promote the degradation and clearance of Aβ aggregates. Furthermore, the physicochemical properties of PBPT are also favorable for CNS permeation. Collectively, these properties highlight the potential of PBPT as a lead compound of the BPT series that possesses promising multi-functional activity to treat the complex pathology associated with AD.

4. Materials and Methods

4.1 Chemicals and Instrumentation

Chemicals used for synthesis were procured from Sigma-Aldrich (St. Louis, MO, USA) and were of the highest quality available and used without further purification. ^{1}H NMR (400 MHz) and ^{13}C NMR (100 MHz) spectra were obtained on a Bruker Advance 400 NMR spectrometer using DMSO-d_6 as a solvent. The following abbreviations are used to describe peak multiplicities: s, singlet; d, doublet; t, triplet; dd, doublet of doublet; td, triplet of doublet, bs, broad singlet; bd, broad doublet; m, multiplet. Moreover, the following abbreviations were used to label different protons: CH_2-pip, piperidine, CH_2-benzyl, benzylic; CH-phenyl, phenyl; CH-pyridox, pyridoxal; CH-sal, salicylyl; CH-naph, naphthyl; CH-quin, quinonyl; CH-Bz, benzaldehyde. Biochemicals, including MTT, protease (*i.e.*, Pronase) from *Streptomyces griseus* and human Tf, were purchased from Sigma-Aldrich. Electrospray ionization mass spectrometry (ESI-MS) measurements were carried out on a Bruker amaZon SL mass spectrometer in enhanced resolution mode. All UV-visible spectra were acquired using a Shimadzu UV-1800 spectrophotometer. Elemental analysis was performed on a Thermo Scientific Flash 2000 CHNS/O analyzer. The purity of all ligands and their copper and iron complexes were assessed by elemental analysis (C, H, N, S) and determined to be ≥95%.

4.2 Synthesis of 4-(1-benzylpiperidin-4-yl)thiosemicarbazide

The precursor, 4-(1-benzylpiperidin-4-yl)thiosemicarbazide, was synthesized using a standard procedure [50]. To an aqueous solution (100 mL) containing sodium hydrazide (1.0 g, 25.0 mmol), carbon disulfide (2.0 g, 26.3 mmol) was added, followed by 4-amino-1-benzylpiperidine (4.65 g, 24.4 mmol) and the mixture stirred at RT. The solution turned to a yellow-orange color and the organic layer slowly disappeared over time. After 4 h, sodium chloroacetate (3.05 g, 26.2 mmol) was added and stirred for another 15 h at RT. Upon the addition of concentrated HCl (3 mL) to the reaction mixture, a precipitate formed, which was subsequently reacted with hydrazine hydrate

(2.50 g, 50 mmol) at 90°C for 2 h and cooled to RT. The subsequent white precipitate that formed was collected by filtration, washed with water and air dried. This afforded 3.9 g of 4-(1-benzylpiperidin-4-yl)thiosemicarbazide as a white solid. Overall yield: 60%. ^{1}H NMR: δ ppm (DMSO-d_6) 1.51 (2H, m, CH_2-pip), 1.81 (2H, m, CH_2-pip), 2.04 (2H, m, CH_2-pip), 2.73 (2H, bd, CH_2-pip), 3.45 (2H, s, CH_2-benzyl), 4.09 (1H, m, CH-NH), 4.46 (2H, s, NH_2), 7.27 (5H, m, 5×CH-phenyl), 7.56 (1H, d, J = 8.2 Hz, NH-CH), 8.61 (1H, s, NH-N). ^{13}C NMR: δ ppm (DMSO-d_6) 32.0, 50.5, 52.5, 62.6, 127.3, 128.6, 129.2, 139.0, 180.7.

4.3 General procedure for the preparation of the novel BPT ligands

A solution of 4-(1-benzylpiperidin-4-yl)thiosemicarbazide (0.53 g, 2.0 mmol) in ethanol (15 mL) was refluxed with an equimolar amount of various aldehydes for 2 h in the presence of a few drops of glacial acetic acid. The precipitate that formed after cooling to room temperature was collected by filtration and washed with adequate amounts of ethanol and dried.

Pyridoxal 4-(1-benzylpiperidin-4-yl)thiosemicarbazone (PBPT)

Yellow solid (0.82 g). Yield: 91%. ^{1}H NMR: δ ppm (DMSO-d_6) 1.98 (2H, m, CH_2-pip), 2.09 (2H, m, CH_2-pip), 2.42 (3H, s, CH_3), 3.02 (2H, bs, CH_2-pip), 3.30 (2H, bs, CH_2-pip), 4.23 (2H, bs, CH_2-Ph), 4.37 (1H, bs, CH-NH), 4.57 (2H, s, CH_2-OH), 5.34 (1H, bs, CH_2-OH), 7.45 (3H, m, 3×CH-phenyl), 7.61 (2H, d, J = 3.3 Hz, 2×CH-phenyl), 7.97 (1H, s, CH-pyridoxal), 8.56 (1H, s, CH=N), 8.72 (1H, bs, NH-CH), 10.89 (1H, bs, OH), 11.82 (1H, bs, NH-N). ^{13}C NMR: δ ppm (DMSO-d_6) 19.6, 28.5, 50.0, 50.9, 59.5, 129.2, 129.7, 131.7, 133.0, 139.6, 141.7, 147.6, 149.6, 152.9, 178.0. ESI-MS in CH_3CN: found mass: 414.21 (100%), Calc. mass for $C_{21}H_{28}N_5O_2S$: 414.20 $[M+H^+]^+$. Anal. Calc. for $C_{21}H_{27}N_5O_2S\cdot(HCl)(H_2O)_2(CH_3COOH)_{0.5}$ (%): C 51.20, H 6.64, N 13.57, S 6.21. Found (%): C 51.31, H 6.74, N 13.76, S 6.16.

Salicylaldehyde 4-(1-benzylpiperidin-4-yl)thiosemicarbazone (SBPT)

White solid (0.69 g). Yield: 94%. ^{1}H NMR: δ ppm (DMSO-d_6) 1.74 (2H, m, CH_2-pip), 1.81 (2H, m, CH_2-pip), 2.03 (2H, m, CH_2-pip), 2.80 (2H, bd, CH_2-pip), 3.40 (2H, s, CH_2-benzyl), 4.24 (1H, m, CH-NH), 6.84 (2H, m, 2×CH-sal), 7.22 (2H, m, 2×CH-sal,phenyl), 7.32 (4H, m, 4×CH-phenyl), 7.93 (1H, d, *J* = 7.8 Hz, CH-sal), 8.03 (1H, d, *J* = 8.6 Hz, NH-CH), 8.38 (1H, s, CH=N), 9.96 (1H, bs, OH), 11.38 (1H, s, NH-N). ^{13}C NMR: δ ppm (DMSO-d_6) 31.5, 51.5, 52.7, 62.5, 116.5, 119.7, 120.8, 127.2, 127.3, 128.6, 129.2, 131.5, 139.1, 139.9, 156.9, 176.3. ESI-MS in CH_3CN: found mass: 369.17 (100%), Calc. mass for $C_{20}H_{25}N_4OS$: 369.18 $[M+H^+]^+$. Anal. Calc. for $C_{20}H_{24}N_4OS \cdot CH_3COOH$ (%): C 61.66, H 6.59, N 13.07, S 7.48. Found (%): C 61.82, H 6.48, N 13.28, S 7.36.

2-Hydroxy-1-naphthaldehyde 4-(1-benzylpiperidin-4-yl)thiosemicarbazone (NBPT)

Yellow solid (0.78 g). Yield: 93%. ^{1}H NMR: δ ppm (DMSO-d_6) 1.67 (2H, m, CH_2-pip), 1.88 (2H, m, CH_2-pip), 2.10 (2H, m, CH_2-pip), 2.75 (2H, bd, CH_2-pip), 3.48 (2H, s, CH_2-benzyl), 4.25 (1H, m, CH-NH), 7.21 (1H, d, *J* = 8.9 Hz, CH-naph), 7.26 (1H, m, CH-phenyl), 7.31 (4H, m, 4×CH-phenyl), 7.39 (1H, t, *J* = 7.5 Hz, CH-naph), 7.57 (1H, m, CH-naph), 7.88 (2H, m, 2×CH-naph), 8.03 (1H, d, *J* = 8.1 Hz, NH-CH), 8.46 (1H, d, *J* = 8.6 Hz, CH-naph), 9.03 (1H, s, CH=N), 10.64 (1H, bs, OH), 11.43 (1H, s, NH-N). ^{13}C NMR: δ ppm (DMSO-d_6) 31.4, 51.4, 52.4, 62.6, 110.4, 118.9, 123.0, 123.9, 127.3, 128.2, 128.6, 128.7, 129.2, 129.3, 132.0, 132.8, 139.0, 142.9, 156.9, 176.3. ESI-MS in CH_3CN: found mass: 419.18 (100%), Calc. mass for $C_{24}H_{27}N_4OS$: 419.19 $[M+H^+]^+$. Anal. Calc. for $C_{24}H_{26}N_4OS$ (%): C 68.87, H 6.26, N 13.39, S 7.66. Found (%): C 68.83, H 6.28, N 13.60, S 7.56.

2-Pyridinecarboxaldehyde 4-(1-benzylpiperidin-4-yl)thiosemicarbazone (PCBPT)

White solid (0.75 g). Yield: 50%. X-ray diffraction quality crystals were obtained from ethanol by slow evaporation. ^{1}H NMR: δ ppm (DMSO-d_6) 1.77 (4H, m, 2×CH_2-pip), 2.02 (2H, m, CH_2-pip),

2.82 (2H, bd, CH_2-pip), 3.18 (2H, s, CH_2-benzyl), 4.27 (1H, m, CH-NH), 7.25 (1H, m, CH-phenyl), 7.33 (4H, m, 4×CH-phenyl), 7.39 (1H, m, CH-pyr), 7.84 (1H, td, *J* = 7.8, 1.6 Hz, CH-pyr), 8.11 (1H, s, CH=N), 8.25 (1H, d, *J* = 8.5 Hz, CH-pyr), 8.30 (1H, d, J = 8.1 Hz, NH-CH), 8.57 (1H, d, *J* = 4.4 Hz, CH-pyr), 11.66 (1H, s, NH-N). ^{13}C NMR: δ ppm (DMSO-d_6) 31.3, 51.8, 52.7, 62.5, 120.9, 124.6, 127.3, 128.6, 129.1, 136.9, 139.2, 143.0, 149.8, 153.7, 176.7. ESI-MS in CH_3CN: found mass: 354.17 (100%), Calc. mass for $C_{19}H_{24}N_5S$: 354.17 $[M+H^+]^+$. Anal. Calc. for $C_{19}H_{23}N_5S\cdot(H_2O)_{0.25}$ (%): C 63.74, H 6.62, N 19.56, S 8.96. Found (%): C 63.55, H 6.48, N 19.78, S 8.84.

2-Quinolinecarboxaldehyde 4-(1-benzylpiperidin-4-yl)thiosemicarbazone (QBPT)

Yellow solid (1.1 g). Yield: 63%. Single crystals suitable for X-ray diffraction were obtained from the mother liquor, ethanol. ^{1}H NMR: δ ppm (DMSO-d_6) 1.76-1.85 (4H, m, 2×CH_2-pip), 2.03 (2H, m, CH_2-pip), 2.86 (2H, bd, CH_2-pip), 3.49 (2H, s, CH_2-benzyl), 4.30 (1H, m, CH-NH), 7.26 (1H, m, CH-phenyl), 7.32 (4H, m, 4×CH-phenyl), 7.63 (1H, m, CH-quin), 7.78 (1H, td, *J* = 7.2, 1.2 Hz, CH-quin), 8.01 (2H, m, 2×CH-quin), 8.26 (1H, s, CH=N), 8.40 (2H, m, 2×CH-quin), 8.47 (1H, d, *J* = 8.8 Hz, NH-CH), 11.83 (1H, s, NH-N). ^{13}C NMR: δ ppm (DMSO-d_6) 31.3, 52.0, 52.8, 62.5, 118.7, 127.3, 127.6, 128.3, 128.4, 128.6, 129.2, 129.3, 130.4, 136.7, 139.2, 143.1, 147.8, 154.3, 176.7. ESI-MS in CH_3CN: found mass: 404.19 (100%), Calc. mass for $C_{23}H_{26}N_5S$: 404.19 $[M+H^+]^+$. Anal. Calc. for $C_{23}H_{25}N_5S$ (%): C 68.46, H 6.24, N 17.35, S 7.94. Found (%): C 68.34, H 6.26, N 17.53, S 7.82.

8-Hydroxy-2-quinolinecarboxaldehyde 4-(1-benzylpiperidin-4-yl)thiosemicarbazone (8-OH-QBPT)

Yellow solid (1.37 g). Yield: 69%. ^{1}H NMR: δ ppm (DMSO-d_6) 1.79-1.85 (4H, m, 2×CH_2-pip), 2.03 (2H, m, CH_2-pip), 2.84 (2H, bd, CH_2-pip), 3.49 (2H, s, CH_2-benzyl), 4.31 (1H, m, CH-NH), 7.11 (1H, dd, *J* = 7.2, 1.6 Hz, CH-quin), 7.26 (1H, m, CH-phenyl), 7.33 (4H, m, 4×CH-phenyl),

7.42 (2H, m, 2×CH-quin), 8.29 (1H, s, CH=N), 8.31 (H, d, CH-quin), 8.38 (1H, d, *J* = 8.5 Hz, CH-quin), 8.46 (1H, d, J = 8.5 Hz, NH-CH), 9.83 (1H, s, OH), 11.88 (1H, s, NH-N). ^{13}C NMR: δ ppm (DMSO-d_6) 31.3, 51.9, 52.8, 62.5, 112.6, 118.3, 119.0, 127.3, 128.5, 128.6, 129.2, 129.3, 136.5, 138.7, 139.2, 142.9, 152.2, 153.9, 176.7. ESI-MS in CH_3CN: found mass: 420.18 (100%), Calc. mass for $C_{23}H_{26}N_5OS$: 420.19 $[M+H^+]^+$. Anal. Calc. for $C_{23}H_{25}N_5OS$ (%): C 65.85, H 6.01, N 16.69, S 7.64. Found (%): C 65.80, H 6.00, N 16.79, S 7.49.

2,3-Dihydroxybenzaldehyde 4-(1-benzylpiperidin-4-yl)thiosemicarbazone (2,3-OH-BBPT)

White crystals (0.68 g). Yield: 88%. ^{1}H NMR: δ ppm (DMSO-d_6) 1.72 (2H, m, CH_2-pip), 1.81 (2H, m, CH_2-pip), 2.03 (2H, m, CH_2-pip), 2.79 (2H, bd, CH_2-pip), 3.48 (2H, s, CH_2-benzyl), 4.22 (1H, m, CH-NH), 6.66 (1H, t, *J* = 7.8 Hz, CH-Bz), 6.80 (1H, dd, *J* = 7.8, 1.4 Hz, CH-Bz), 7.25 (1H, m, CH-Bz), 7.31-7.37 (5H, m, 5×CH-phenyl), 8.01 (1H, d, *J* = 8.4 Hz, NH-CH), 8.38 (1H, s, CH=N), 9.26 (2H, bs, 2×OH), 11.38 (1H, s, NH-N). ^{13}C NMR: δ ppm (DMSO-d_6) 31.4, 51.5, 52.7, 62.5, 116.9, 117.7, 119.5, 121.3, 127.3, 128.6, 129.2, 139.1, 140.6, 145.7, 146.0, 176.2. ESI-MS in CH_3CN: found mass: 385.18 (100%), Calc. mass for $C_{20}H_{25}N_4O_2S$: 385.17 $[M+H^+]^+$. Anal. Calc. for $C_{20}H_{24}N_4O_2S \cdot H_2O$ (%): C 59.68, H 6.51, N 13.92, S 7.97. Found (%): C 59.65, H 6.54, N 13.99, S 7.82.

2,3,4-Trihydroxybenzaldehyde 4-(1-benzylpiperidin-4-yl)thiosemicarbazone (2,3,4-OH-BBPT)

Yellowish brown solid (0.65 g). Yield: 81%. ^{1}H NMR: δ ppm (DMSO-d_6) 1.73 (2H, m, CH_2-pip), 1.86 (2H, m, CH_2-pip), 2.24 (2H, bs, CH_2-pip), 2.89 (2H, bd, CH_2-pip), 3.64 (2H, s, CH_2-benzyl), 4.25 (1H, m, CH-NH), 6.35 (1H, d, *J* = 8.5 Hz, CH-Bz), 7.12 (1H, d, *J* = 8.4 Hz, CH-Bz), 7.29-7.36 (6H, m, 5×CH-phenyl, 1×OH), 7.94 (1H, d, *J* = 8.1 Hz, NH-CH), 8.25 (1H, s, CH=N), 9.13 (1H, bs, OH), 11.23 (1H, s, NH-N). ^{13}C NMR: δ ppm (DMSO-d_6) 30.6, 50.8, 52.1, 61.5, 108.2, 113.0, 118.7, 128.1, 128.8, 129.9, 133.2, 142.4, 147.1, 148.8. ESI-MS in CH_3CN: found mass: 401.17 (100%), Calc. mass for $C_{20}H_{25}N_4O_3S$: 401.17 $[M+H^+]^+$. Anal. Calc. for

$C_{20}H_{24}N_4O_3S\cdot(CH_3COOH)_{0.5}(H_2O)_{2.5}$ (%): C 53.05, H 6.57, N 11.78, S 6.74. Found (%): C 53.17, H 6.08, N 12.03, S 6.75.

4.4 X-ray crystallography

Data were collected at 150 K ([HSBPT][OAc] and PCBPT) or 190 K ([Cu(SBPT)Cl_2]) on an Oxford Diffraction Gemini CCD diffractometer with Cu-Kα radiation (1.54184 Å). Data reduction and empirical absorption corrections (multiscan) were carried out using Oxford Diffraction CrysAlisPro Software. The structures were solved by direct methods with SHELX-86 and refined by full matrix least-squares on F^2 with SHELXL-97 [94,95]. All non-hydrogen atoms were refined anisotropically and hydrogen atoms were fixed in their calculated positions using a riding model. Molecular structure diagrams were generated with ORTEP3 [96] and rendered with PovRay (version 3.7). Crystal data in CIF format have been deposited with the Cambridge Crystallographic Data Centre (CCDC numbers: 1516075, 1516076 and 1516077 for [Cu(SBPT)Cl_2], [HSBPT][OAc] and PCBPT, respectively).

4.5 Cyclic Voltammetry and EPR Spectroscopy

Cyclic voltammetry measurements were performed using a BAS100B/W potentiostat in a three electrode cell set-up with a glassy carbon working electrode, Ag/AgCl reference electrode and Pt wire auxiliary electrode. The working electrode was polished using 0.5 µm alumina and then rinsed thoroughly with Milli-Q water prior to each measurement. The data were collected for all complexes in an aqueous buffer (50 mM Tris buffer and 0.1 M NEt_4ClO_4) containing DMF (70:30 v/v) with all complexes at a concentration of 1 mM. All potentials are reported *versus* the NHE by correction of the potentials measured with respect to the Ag/AgCl reference (calibrated with quinhydrone at pH 7). Electron paramagnetic resonance (EPR) spectra were collected on a Bruker ER200 instrument at X-band frequency (9.370 GHz) in 1 mM DMF frozen solutions at 130 K.

4.6 Cell Culture

Human SK-N-MC neuroepithelioma cells were obtained from the American Type Culture Collection (ATCC; Vanassas, VI, USA) and cultured in complete minimum essential medium (MEM; Sigma-Aldrich) containing 10% fetal calf serum (FSC; Sigma-Aldrich); 0.28 µg/mL fungizone; 100 U/mL penicillin; 1% MEM non-essential amino acids; 1% sodium pyruvate; and 1% glutamine (Life Technologies; California, USA) at 37°C in a humidified atmosphere containing 5% CO_2 and 95% air. Cells were subcultured and implemented for further experiments using standard procedures [43,61].

4.7 Cellular Proliferation Assay

The cytotoxicity of the BPT series against SK-N-MC cells was determined using the [1-(4,5-dimethylthiazol-2-yl)-2,5-diphenyl tetrazolium] (MTT) assay using standard techniques [61]. The cells were seeded in 96-well microtiter plates at a density of 1.5×10^4 cells/well. The compounds were dissolved in DMSO (20 mM) and diluted further using MEM media to result in a final concentration of DMSO ≤0.5% (v/v). At this concentration, DMSO has no effect on cellular proliferation [61]. After 24 h, the cells were exposed to various concentrations of chelators or their copper or iron complexes (0–100 µM) and incubated for 72 h at 37°C. After this incubation, 20 µL of MTT (5 mg/mL in PBS) was added to each well and incubated further for 2 h/37°C. Culture medium was aspirated carefully and 100 µL of DMSO was added to dissolve the formazan crystals. The plates were shaken for 5 min and the absorbance was measured at 570 nm using a scanning multi-well spectrophotometer. The half maximal inhibitory concentration (IC_{50}) was defined as the chelator concentration necessary to reduce the absorbance to 50% of the untreated control [61]. Control studies demonstrated that absorbance at 570 nm was proportional to the number of viable cells as determined by direct cell counts using Trypan blue [61].

4.8 Labeling of Transferrin with ^{59}Fe

Apo-transferrin (ApoTf; Sigma-Aldrich) was labeled with ^{59}Fe (PerkinElmer Life Sciences, Waltham, MA) and then purified by standard methodology using dialysis to generate diferric Tf ($^{59}Fe_2$-Tf) [97,98].

4.9 Effect of the BPT Analogues on Iron Efflux from SK-N-MC cells

The effect of BPT compounds on ^{59}Fe mobilization from SK-N-MC cells was determined by ^{59}Fe efflux experiments using a standard protocol [99]. Briefly, SK-N-MC cells were seeded in 6-well plates and incubated overnight. The cell growth medium was aspirated and then the cells prelabeled with $^{59}Fe_2$-Tf (0.75 μM) in complete medium (1 mL) for 3 h at 37°C. Cells were washed four times with ice-cold PBS to remove extracellular $^{59}Fe_2$-Tf and then incubated for 3 h at 37°C with medium alone (control) or medium containing the BPT compounds (25 μM). The well characterized chelators, Dp44mT (25 μM) and DFO (25 μM), and the AD therapeutic, Donepezil (25 μM), were included as controls. After the incubation, cells were placed on ice and the media containing released ^{59}Fe was separated from the monolayer using a pasteur pipette. Subsequently, PBS (1 mL) was added to the cells and then the monolayer removed using a plastic spatula. Radioactivity was measured in both the cell suspension and supernatant using a γ-scintillation counter (Wallac Wizard 3, PerkinElmer, Waltham, MA).

4.10 Effect of the BPT Analogues on Iron Uptake from $^{59}Fe_2$-Tf by SK-N-MC Cells

In order to estimate the ability of novel BPT compounds to prevent the cellular uptake of ^{59}Fe from the Fe transport protein, $^{59}Fe_2$-Tf, ^{59}Fe uptake experiments were performed using standard procedures [61,67]. Briefly, SK-N-MC cells were incubated with $^{59}Fe_2$-Tf (0.75 μM) and the compounds (25 μM) in complete medium for 3 h at 37℃. The medium was then removed and cells washed four times with ice-cold PBS to remove excess extracellular $^{59}Fe_2$-Tf. Subsequently, cells were incubated with the protease, pronase (1 mg/mL; Sigma-Aldrich), for 30 min/4°C to separate

internalized from membrane-bound ^{59}Fe using a well-established protocol [97,100]. The monolayer of cells was then detached from the substratum using a plastic spatula and centrifuged at 10,000 rpm for 3 min/4°C. The supernatant media that contained membrane-bound ^{59}Fe was removed and placed in a γ-counting tube and the pellet containing internalized ^{59}Fe was resuspended in 1 mL of PBS and added to a separate γ-counting tube. The ^{59}Fe levels in both the supernatant and cell pellet were measured on the γ-scintillation counter described above. As utilized in ^{59}Fe efflux experiments, Dp44mT (25 µM), DFO (25 µM) and Donepezil (25 µM) were included as controls.

4.11 Effect of the BPT Analogues on Ascorbate Oxidation

The ability of the iron complexes of the BPT compounds to catalyze the oxidation of ascorbate was examined as previously described [69]. The assay was carried out in disodium hydrogen phosphate buffer (10 mM; pH = 7.4) containing 10% (v/v) acetonitrile and sodium citrate (500 µM). Freshly prepared sodium ascorbate (50 µM) was incubated with $FeCl_3$ alone (10 µM, control), or in the presence of chelators at an iron-binding equivalent (IBE) of 1. This IBE results in a fully occupied Fe(III) coordination sphere upon complexation (*e.g.*, Fe(III)–EDTA (1:1 ratio), Fe(III)–DFO (1:1 ratio), Fe(III)–Dp44mT (1:2 ratio), Fe(III)–Donepezil (1:2 ratio), and Fe(III)–BPT analogues (1:2 ratio). In these studies, ethylenediaminetetraacetic acid (EDTA), Dp44mT, DFO and Donepezil were included as controls. Furthermore, while Donepezil is not a chelator, Fe(III) was added at a 1:2 ratio for comparison purposes to the thiosemicarbazones. The absorbance at 265 nm was measured using UV-visible spectrophotometer after 10 and 40 min of incubation at RT and the decrease in absorbance between the two time points was calculated and expressed as a percentage of ascorbate oxidation relative to the control (100%).

4.12 Protection against Hydrogen Peroxide-Mediated Cytotoxicity

The ability of the novel BPT agents to protect SK-N-MC neuroepithelioma cells against H_2O_2-mediated cytotoxicity was assessed using the MTT assay following previously reported protocols

with slight alterations [74,101]. SK-N-MC cells were seeded in 96-well microtiter plates at a density of 1.5×10^4 cells/well and incubated at 37°C/24 h. After this period, the cells were pre-incubated for 2 h/37°C with serum-free medium alone (control), the BPT ligands, or the relevant controls, including DFO and Donepezil, at 10 μM (final DMSO concentration ≤0.2% v/v) in serum-free medium. The medium was then removed and the cells incubated with fresh serum-free medium alone, or serum-free medium containing H_2O_2 (150 μM), for a further 24 h/37°C. The cellular viability was then measured as described above using the MTT assay.

4.13 Effect of the BPT Analogues on Acetylcholinesterase Activity

Studies examining the ability of the novel agents to inhibit AChE were performed using established procedures with slight modifications [102,103]. Acetylthiocholine iodide (Sigma-Aldrich) was used as a substrate in this assay and is metabolized by AChE (from *Electrophorus electricus*; Sigma-Aldrich) to produce thiocholine [104]. This product subsequently reacts with 5,5'-dithio-bis-(2-nitrobenzoic acid) (DTNB) to generate a yellow product, 5-thio-2-nitrobenzoic acid, which is detected spectrophotometrically at 405 nm [104]. Stock solutions of the BPT ligands (200-times higher than the final concentration) were prepared in DMSO. In this study, Donepezil and Tacrine were used as positive controls due to their well characterized ability to potently inhibit AChE [76]. The working solutions were prepared by dissolving 12.5 μL of BPT analogues or DMSO (control) in 1022 μL of HEPES buffer (50 mM; NaCl 150 mM; $MgCl_2$ 20 mM; pH 8.0).

The working solution of a compound (207 μL) was added to a cuvette containing 238 μL of DTNB (3 mM in HEPES buffer) and 37.5 μL of AChE at a concentration of 0.26 U/mL and incubated for 15 min at room temperature. The enzymatic reaction was initiated by the addition of 37.5 μL of acetylthiocholine iodide (15 mM in HEPES buffer). The solution was immediately analyzed at 405 nm on Shimadzu UV-1800 spectrophotometer (Kyoto, Kyoto Prefecture, Japan) in kinetic mode for 5 min. The final concentration of DMSO was maintained at 0.5% throughout the studies. The

percentage of activity was calculated using the equation: % Activity = 100 - (slope of sample/slope of DMSO control).

4.14 Molecular Docking

Molecular computational docking was completed using Grid-based Ligand Docking with Energetics (GLIDE; Schrödinger; New York, USA) software. The active site of the human AChE protein (PDB ID: 4EY7; 2.35 Å) was prepared *via* the Protein Preparation Wizard embedded in Maestro v11.1.012 (Schrödinger, LLC, New York, USA). Protein preparation was completed by using default settings such as the addition of hydrogen and disulfide bonds, and the removal of waters beyond 5 Å. The protein was further reviewed and modified by deleting additional ligands. The protein was prepared at pH 7 ± 3. The BPT ligands were optimized using the LigPrep (Schrödinger) and GonfGen (Schrödinger) modules to generate multiple stable conformations of the ligands in three-dimension. These conformations were docked onto the active site of AChE. The GLIDE XP docking score was generated to estimate the ligand binding free energy taking into account the EPIK state penalty [105]. Molecular dynamics simulation-based molecular mechanics generalized born surface area (MM-GBSA; Schrödinger) was performed to estimate the relative binding affinity between the ligand and protein target.

4.15 Effect of the BPT Analogues on Inhibition of Cu(II)-Mediated $A\beta_{1-40}$ Aggregation

An established turbidity assay was used to evaluate the potential of the BPT ligands to inhibit the aggregation induced by Cu(II) [47,83,84]. Briefly, 1 mg of synthetic human $A\beta_{1–40}$ purchased from ChinaPeptides (Shanghai, China) was dissolved in 50 μL of DMSO and then 910 μL of Milli-Q water was added just prior the experiment to provide a solution of 250 μM. Stock solutions of agents, including DTPA, Dp44mT, Donepezil, Tacrine and the BPT analogues, were prepared in DMSO (10 mM) and diluted further with HEPES buffer (20 mM HEPES, 150 mM NaCl, pH 6.6). This solution was passed through Chelex resin to remove trace metal ions and filtered using a 0.2

μm filter to achieve a working stock of 250 μM. A stock solution (250 μM) of $CuCl_2$ (analytical grade, Sigma-Aldrich) was also prepared in HEPES buffer. Solutions of Cu(II) (5 μL) and $A\beta_{1-40}$ (5 μL) were added to HEPES buffer (35 μL) in the 384-well plate, which was then incubated with the ligands (5 μL) in a final volume of 50 μL in quadruplicates. The final concentrations of the ligands, Cu(II) and $A\beta_{1-40}$ were 25 μM each. The solutions were incubated for 2 h/37 °C and absorbance measured at 405 nm using a FluoStar Omega Plate Reader (BMG Labtech, Ortenberg, Germany). The absorbance of Cu(II), the ligand and buffer were used as blanks and subtracted from corresponding wells. Both Cu(II) and peptide were used alone as positive controls to demonstrate the effect on peptide aggregation in the absence of the ligand.

4.16 Western blotting

Western blotting was performed by standard methodology, as previously described [89,106]. Briefly, proteins were separated by SDS-PAGE using the MiniProtein Tetra Cell System (Bio-Rad; CA, USA). After electrophoresis, the gel was electroblotted overnight at 30 V/4^{o}C onto a polyvinylidene difluoride (PVDF) membrane (0.45 μm pore size; GE Healthcare; WI, USA) in 1x transfer buffer. PVDF was activated by 100% methanol and soaked in 1x transfer buffer prior to transfer.

The primary antibodies used for immunoblotting were LC3 (Cat. #: MBPM036; 1:2,000 dilution; Abacus), p62 (Cat. #: ab56416; 1:5,000 dilution; Abcam) and β-actin (Cat. #: A1978; 1:10,000; Sigma). The secondary antibodies used included horseradish peroxidase (HRP)–conjugated anti-rabbit (Cat. #: A6154) and anti-mouse (Cat. #: A4416) antibodies from Sigma-Aldrich. Both antibodies were used at a 1:10,000 dilution. PVDF membranes were incubated with Luminata Forte Western HRP substrate (Millipore, Billerica, MA, USA). The signals were detected using a ChemiDoc MP Imaging System (Bio-Rad) and densitometry performed using Quantity One software (Bio-Rad) and normalized to the relative β-actin-loading control.

4.17 Statistical Analysis

All statistical analysis using Student's *t*-test was performed using Microsoft Excel. Results were considered significant when $p < 0.05$.

Supplementary Material: Chemical synthesis and characterization of all copper and iron complexes, ^{1}H & ^{13}C NMR and ESI-MS spectra of all BPT ligands, crystallographic data of [HSBPT][OAc], PCBPT and [Cu(SBPT)Cl_2], X-band EPR spectra and cyclic voltammograms of all copper and iron complexes of the BPT analogues, and inhibition of Cu(II)-mediated aggregation of $A\beta_{1-42}$.

Corresponding Authors

*Danuta S. Kalinowski, Email: danuta.kalinowski@sydney.edu.au. Phone: +61 2 9351 8976; Des R. Richardson, Email: d.richardson@med.usyd.edu.au; Phone: +61-2-9036-6548

Author Contributions

D.P., R.P., S.S., D.H., H.Y.L., P.V.B. and D.S.K. performed the experiments and contributed to writing the manuscript; R.A performed studies; D.S.K. and D.R.R. conceived the study, designed experiments, obtained research funding and wrote the manuscript. D.S.K. and D.R.R. contributed equally as senior authors.

Conflict of Interest

D.P., R.P., D.S.K. and D.R.R. are co-inventors of a Provisional Patent (AU2016902445) that includes these agents.

Acknowledgments

This work was supported by a Project Grant from the National Health and Medical Research Council (NHMRC) Australia to D.R.R. [1021607] and D.S.K. [1048972]; a NHMRC Senior Principal Research Fellowship to D.R.R. [1062607]; a NHMRC RD Wright Fellowship to D.S.K. [1083057]; and Australian Research Council grants to P.V.B. [DP1096029, DP150104672,

DP150103345, DP1211465]. D.P. thanks the Sydney Medical School for an Early Career Research Grant. D.R.R. and D.S.K. appreciate the award of a Judith Jane Mason and Harold Stannett Williams Memorial Foundation National Medical Program Grant. S.S. thanks Cancer Australia and Cure Cancer Australia for a Young Investigator Priority driven Collaborative Cancer Research Scheme (PdCCRS) Project Grant. We kindly thank Ms. Zhixuan (Zoey) Wu, Molecular Pharmacology and Pathology Program (University of Sydney), for technical assistance in some proliferation assays.

References

[1] M.C. Carreiras, E. Mendes, M.J. Perry, A.P. Francisco, J. Marco-Contelles, The multifactorial nature of Alzheimer's disease for developing potential therapeutics, Curr. Top. Med. Chem. 13 (2013) 1745-1770.

[2] Y.D. Huang, L. Mucke, Alzheimer mechanisms and therapeutic strategies, Cell 148 (2012) 1204-1222.

[3] G.W. Van Hoesen, B.T. Hyman, A.R. Damasio, Entorhinal cortex pathology in Alzheimer's disease, Hippocampus 1 (1991) 1-8.

[4] C.P. Ferri, M. Prince, C. Brayne, H. Brodaty, L. Fratiglioni, M. Ganguli, K. Hall, K. Hasegawa, H. Hendrie, Y.Q. Huang, A. Jorm, C. Mathers, P.R. Menezes, E. Rimmer, M. Scazufca, A.D. Intl, Global prevalence of dementia: a Delphi consensus study, Lancet 366 (2005) 2112-2117.

[5] P.T. Francis, A.M. Palmer, M. Snape, G.K. Wilcock, The cholinergic hypothesis of Alzheimer's disease: a review of progress, J. Neurol. Neurosurg. Psychiatry 66 (1999) 137-147.

[6] S. Ayton, P. Lei, A.I. Bush, Metallostasis in Alzheimer's disease, Free Radic. Biol. Med. 62 (2013) 76-89.

[7] F.M. LaFerla, S. Oddo, Alzheimer's disease: Abeta, tau and synaptic dysfunction, Trends Mol. Med. 11 (2005) 170-176.

[8] K.J. Barnham, C.L. Masters, A.I. Bush, Neurodegenerative diseases and oxidative stress, Nat. Rev. Drug Discov. 3 (2004) 205-214.

[9] R.A. Nixon, Autophagy, amyloidogenesis and Alzheimer disease, J. Cell Sci. 120 (2007) 4081-4091.

[10] P.J. Whitehouse, D.L. Price, R.G. Struble, A.W. Clark, J.T. Coyle, R.D. Mahlon, Alzheimer's disease and senile dementia: loss of neurons in the basal forebrain, Science 215 (1982) 1237-1239.

[11] J.T. Coyle, D.L. Price, M. DeLong, Alzheimer's disease: a disorder of cortical cholinergic innervation, Science 219 (1983) 1184-1190.

[12] J.C. Vickers, T.C. Dickson, P.A. Adlard, H.L. Saunders, C.E. King, G. McCormack, The cause of neuronal degeneration in Alzheimer's disease, Prog. Neurobiol. 60 (2000) 139-165.

[13] D. Fotiou, A. Kaltsatou, D. Tsiptsios, M. Nakou, Evaluation of the cholinergic hypothesis in Alzheimer's disease with neuropsychological methods, Aging Clin. Exp. Res. 27 (2015) 727-733.

[14] C.C. Tan, J.T. Yu, H.F. Wang, M.S. Tan, X.F. Meng, C. Wang, T. Jiang, X.C. Zhu, L. Tan, Efficacy and safety of donepezil, galantamine, rivastigmine, and memantine for the treatment of Alzheimer's disease: a systematic review and meta-analysis, J. Alzheimers Dis. 41 (2014) 615-631.

[15] D. Galimberti, E. Scarpini, Old and new acetylcholinesterase inhibitors for Alzheimer's disease, Expert. Opin. Investig. Drugs 25 (2016) 1-7.

[16] P. Anand, B. Singh, A review on cholinesterase inhibitors for Alzheimer's disease, Arch. Pharm. Res. 36 (2013) 375-399.

[17] A. Budimir, Metal ions, Alzheimer's disease and chelation therapy, Acta Pharm. Sin. B. 61 (2011) 1-14.

[18] W.H. Huang, W.H. Wei, Z.R. Shen, Drug-like chelating agents: a potential lead for Alzheimer's disease, RSC Adv. 4 (2014) 52088-52099.

[19] M.A. Lovell, J.D. Robertson, W.J. Teesdale, J.L. Campbell, W.R. Markesbery, Copper, iron and zinc in Alzheimer's disease senile plaques, J. Neurol. Sci. 158 (1998) 47-52.

[20] A. Yamamoto, R.W. Shin, K. Hasegawa, H. Naiki, H. Sato, F. Yoshimasu, T. Kitamoto, Iron (III) induces aggregation of hyperphosphorylated tau and its reduction to iron (II) reverses the aggregation: implications in the formation of neurofibrillary tangles of Alzheimer's disease, J. Neurochem. 82 (2002) 1137-1147.

[21] M.L. Hegde, P. Bharathi, A. Suram, C. Venugopal, R. Jagannathan, P. Poddar, P. Srinivas, K. Sambamurti, K.J. Rao, J. Scancar, L. Messori, L. Zecca, P. Zatta, Challenges associated with metal chelation therapy in Alzheimer's disease, J. Alzheimers Dis. 17 (2009) 457-468.

[22] D.R.C. Mclachlan, A.J. Dalton, T.P.A. Kruck, M.Y. Bell, W.L. Smith, W. Kalow, D.F. Andrews, Intramuscular desferrioxamine in patients with Alzheimers disease, Lancet 337 (1991) 1304-1308.

[23] P.A. Adlard, R.A. Cherny, D.I. Finkelstein, E. Gautier, E. Robb, M. Cortes, I. Volitakis, X. Liu, J.P. Smith, K. Perez, K. Laughton, Q.X. Li, S.A. Charman, J.A. Nicolazzo, S. Wilkins, K. Deleva, T. Lynch, G. Kok, C.W. Ritchie, R.E. Tanzi, R. Cappai, C.L. Masters, K.J. Barnham, A.I. Bush, Rapid restoration of cognition in Alzheimer's transgenic mice with 8-hydroxy quinoline analogs is associated with decreased interstitial Abeta, Neuron 59 (2008) 43-55.

[24] E.L. Sampson, L. Jenagaratnam, R. McShane, Metal protein attenuating compounds for the treatment of Alzheimer's dementia, Cochrane Database Syst. Rev. (2014) CD005380.

[25] D.M. Wolfe, J.H. Lee, A. Kumar, S. Lee, S.J. Orenstein, R.A. Nixon, Autophagy failure in Alzheimer's disease and the role of defective lysosomal acidification, Eur. J. Neurosci. 37 (2013) 1949-1961.

[26] L.G. Friedman, Y.H. Qureshi, W.H. Yu, Promoting autophagic clearance: viable therapeutic targets in Alzheimer's disease, Neurotherapeutics 12 (2015) 94-108.

[27] P. Nilsson, K. Loganathan, M. Sekiguchi, Y. Matsuba, K. Hui, S. Tsubuki, M. Tanaka, N. Iwata, T. Saito, T.C. Saido, Abeta secretion and plaque formation depend on autophagy, Cell Rep. 5 (2013) 61-69.

[28] A. Agis-Torres, M. Solhuber, M. Fernandez, J.M. Sanchez-Montero, Multi-target-directed ligands and other therapeutic strategies in the search of a real solution for Alzheimer's disease, Curr. Neuropharmacol. 12 (2014) 2-36.

[29] F. Prati, A. Cavalli, M.L. Bolognesi, Navigating the chemical space of multitarget-directed ligands: from hybrids to fragments in Alzheimer's disease, Molecules 21 (2016) 466.

[30] Y. Wang, H. Wang, H.Z. Chen, AChE inhibition-based multi-target-directed ligands, a novel pharmacological approach for the symptomatic and disease-modifying therapy of Alzheimer's disease, Curr. Neuropharmacol. 14 (2016) 364-375.

[31] K.S.T. Dias, C. Viegas, Multi-target directed drugs: a modern approach for design of new drugs for the treatment of Alzheimer's disease, Curr. Neuropharmacol. 12 (2014) 239-255.

[32] Y. Li, X.M. Qiang, L. Luo, X. Yang, G.Y. Xiao, Q. Liu, J.C. Ai, Z.H. Tan, Y. Deng, Aurone Mannich base derivatives as promising multifunctional agents with acetylcholinesterase inhibition, anti-beta-amyloid aggragation and neuroprotective properties for the treatment of Alzheimer's disease, Eur. J. Med. Chem. 126 (2017) 762-775.

[33] Z.K. Liu, L. Fang, H. Zhang, S.H. Gou, L. Chen, Design, synthesis and biological evaluation of multifunctional tacrine-curcumin hybrids as new cholinesterase inhibitors with metal ions-chelating and neuroprotective property, Bioorg. Med. Chem. 25 (2017) 2387-2398.

[34] J. Kumar, P. Meena, A. Singh, E. Jameel, M. Maqbool, M. Mobashir, A. Shandilya, M. Tiwari, N. Hoda, B. Jayaram, Synthesis and screening of triazolopyrimidine scaffold as multi-functional agents for Alzheimer's disease therapies, Eur. J. Med. Chem. 119 (2016) 260-277.

[35] K.S.T. Dias, C.T. de Paula, T. dos Santos, I.N.O. Souza, M.S. Boni, M.J.R. Guimaraes, F.M.R. da Silva, N.G. Castro, G.A. Neves, C.C. Veloso, M.M. Coelho, I.S.F. de Melo, F.C.V. Giusti, A. Giusti-Paiva, M.L. da Silva, L.E. Dardenne, I.A. Guedes, L. Pruccoli, F. Morroni, A. Tarozzi, C. Viegas, Design, synthesis and evaluation of novel feruloyl-donepezil hybrids as potential multitarget drugs for the treatment of Alzheimer's disease, Eur. J. Med. Chem. 130 (2017) 440-457.

[36] B. Sameem, M. Saeedi, M. Mahdavi, A. Shafiee, A review on tacrine-based scaffolds as multi-target drugs (MTDLs) for Alzheimer's disease, Eur. J. Med. Chem. 128 (2017) 332-345.

[37] L. Wang, G. Esteban, M. Ojima, O.M. Bautista-Aguilera, T. Inokuchi, I. Moraleda, I. Iriepa, A. Samadi, M.B.H. Youdim, A. Romero, E. Soriano, R. Herrero, A.P.F. Fernandez, Ricardo-Martinez-Murillo, J. Marco-Contelles, M. Unzeta, Donepezil + propargylamine + 8-hydroxyquinoline hybrids as new multifunctional metal-chelators, ChE and MAO inhibitors for the potential treatment of Alzheimer's disease, Eur. J. Med. Chem. 80 (2014) 543-561.

[38] Z.M. Wang, P. Cai, Q.H. Liu, D.Q. Xu, X.L. Yang, J.J. Wu, L.Y. Kong, X.B. Wang, Rational modification of donepezil as multifunctional acetylcholinesterase inhibitors for the treatment of Alzheimer's disease, Eur. J. Med. Chem. 123 (2016) 282-297.

[39] F. Prati, C. Bergamini, R. Fato, O. Soukup, J. Korabecny, V. Andrisano, M. Bartolini, M.L. Bolognesi, Novel 8-hydroxyquinoline derivatives as multitarget compounds for the treatment of Alzheimer's disease, ChemMedChem 11 (2016) 1284-1295.

[40] H.L. Zheng, M.B.H. Youdim, M. Fridkin, Site-activated multifunctional chelator with acetylcholinesterase and neuroprotective-neurorestorative moieties for Alzheimer's therapy, J. Med. Chem. 52 (2009) 4095-4098.

[41] Z. Kovacevic, D.S. Kalinowski, D.B. Lovejoy, Y. Yu, Y. Suryo Rahmanto, P.C. Sharpe, P.V. Bernhardt, D.R. Richardson, The medicinal chemistry of novel iron chelators for the treatment of cancer, Curr. Top. Med. Chem. 11 (2011) 483-499.

[42] Y. Yu, D.S. Kalinowski, Z. Kovacevic, A.R. Siafakas, P.J. Jansson, C. Stefani, D.B. Lovejoy, P.C. Sharpe, P.V. Bernhardt, D.R. Richardson, Thiosemicarbazones from the old to new: iron chelators that are more than just ribonucleotide reductase inhibitors, J. Med. Chem. 52 (2009) 5271-5294.

[43] J. Yuan, D.B. Lovejoy, D.R. Richardson, Novel di-2-pyridyl-derived iron chelators with marked and selective antitumor activity: in vitro and in vivo assessment, Blood 104 (2004) 1450-1458.

[44] M. Whitnall, J. Howard, P. Ponka, D.R. Richardson, A class of iron chelators with a wide spectrum of potent antitumor activity that overcomes resistance to chemotherapeutics, Proc. Natl. Acad. Sci. U.S.A. 103 (2006) 14901-14906.

[45] D.B. Lovejoy, D.R. Richardson, Novel "hybrid" iron chelators derived from aroylhydrazones and thiosemicarbazones demonstrate selective antiproliferative activity against tumor cells, Blood 100 (2002) 666-676.

[46] K.P. Kepp, Bioinorganic chemistry of Alzheimer's disease, Chem. Rev. 112 (2012) 5193-5239.

[47] L.M. Gomes, R.P. Vieira, M.R. Jones, M.C. Wang, C. Dyrager, E.M. Souza-Fagundes, J.G. Da Silva, T. Storr, H. Beraldo, 8-Hydroxyquinoline Schiff-base compounds as antioxidants and modulators of copper-mediated Aβ peptide aggregation, J. Inorg. Biochem. 139 (2014) 106-116.

[48] G. Kryger, I. Silman, J.L. Sussman, Structure of acetylcholinesterase complexed with E2020 (Aricept): implications for the design of new anti-Alzheimer drugs, Structure 7 (1999) 297-307.

[49] J. Cheung, M.J. Rudolph, F. Burshteyn, M.S. Cassidy, E.N. Gary, J. Love, M.C. Franklin, J.J. Height, Structures of human acetylcholinesterase in complex with pharmacologically important ligands, J. Med. Chem. 55 (2012) 10282-10286.

[50] J.P. Scovill, A facile synthesis of thiosemicarbazides and thiosemicarbazones by the transamination of 4-methyl-4-phenyl-3-thiosemicarbazide, Phosphorus Sulfur Silicon Relat. Elem. 60 (1991) 15-19.

[51] M.N.M. Milunovic, E.A. Enyedy, N.V. Nagy, T. Kiss, R. Trondl, M.A. Jakupec, B.K. Keppler, R. Krachler, G. Novitchi, V.B. Arion, L- and D-proline thiosemicarbazone conjugates: Coordination behavior in solution and the effect of copper(II) coordination on their antiproliferative activity, Inorg. Chem. 51 (2012) 9309-9321.

[52] S.I. Orysyk, G.G. Repich, V.V. Bon, V.V. Dyakonenko, V.V. Orysyk, Y.L. Zborovskii, O.V. Shishkin, V.I. Pekhnyo, M.V. Vovk, Novel Fe(III), Co(III), Ni(II), Cu(II) coordination compounds involving 2-[(2-hydroxyphenyl)methylene]hydrazine-N-(2-propenyl)carbothioamide as ligand: synthesis, crystal structures and spectral characteristics, Inorg. Chim. Acta. 423 (2014) 496-503.

[53] A. Dobrova, S. Platzer, F. Bacher, M.N. Milunovic, A. Dobrov, G. Spengler, E.A. Enyedy, G. Novitchi, V.B. Arion, Structure-antiproliferative activity studies on l-proline- and homoproline-4-N-pyrrolidine-3-thiosemicarbazone hybrids and their nickel(II), palladium(II) and copper(II) complexes, Dalton Trans. 45 (2016) 13427-13439.

[54] D.R. Richardson, P.C. Sharpe, D.B. Lovejoy, D. Senaratne, D.S. Kalinowski, M. Islam, P.V. Bernhardt, Dipyridyl thiosemicarbazone chelators with potent and selective antitumor activity form iron complexes with redox activity, J. Med. Chem. 49 (2006) 6510-6521.

[55] D.B. Lovejoy, P.J. Jansson, U.T. Brunk, J. Wong, P. Ponka, D.R. Richardson, Antitumor activity of metal-chelating compound Dp44mT Is mediated by formation of a redox-active copper complex that accumulates in lysosomes, Cancer Res. 71 (2011) 5871-5880.

[56] D.S. Kalinowski, Y. Yu, P.C. Sharpe, M. Islam, Y.T. Liao, D.B. Lovejoy, N. Kumar, P.V. Bernhardt, D.R. Richardson, Design, synthesis, and characterization of novel iron chelators: structure-activity relationships of the 2-benzoylpyridine thiosemicarbazone series and their 3-nitrobenzoyl analogues as potent antitumor agents, J. Med. Chem. 50 (2007) 3716-3729.

[57] D.R. Richardson, D.S. Kalinowski, V. Richardson, P.C. Sharpe, D.B. Lovejoy, M. Islam, P.V. Bernhardt, 2-Acetylpyridine thiosemicarbazones are potent iron chelators and antiproliferative agents: redox activity, iron complexation and characterization of their antitumor activity, J. Med. Chem. 52 (2009) 1459-1470.

[58] K. Plaschke, J. Kopitz, In vitro streptozotocin model for modeling Alzheimer-like changes: effect on amyloid precursor protein secretases and glycogen synthase kinase-3, J. Neural Transm. 122 (2015) 551-557.

[59] A.S.L. Chan, L.W.C. Ng, L.S.W. Poon, W.W.Y. Chan, Y.H. Wong, Dopaminergic and adrenergic toxicities on SK-N-MC human neuroblastoma cells are mediated through G protein signaling and oxidative stress, Apoptosis 12 (2007) 167-179.

[60] D.S. Kalinowski, D.R. Richardson, The evolution of iron chelators for the treatment of iron overload disease and cancer, Pharmacol. Rev. 57 (2005) 547-583.

[61] D.R. Richardson, E.H. Tran, P. Ponka, The potential of iron chelators of the pyridoxal isonicotinoyl hydrazone class as effective antiproliferative agents, Blood 86 (1995) 4295-4306.

[62] Z. Al-Eisawi, C. Stefani, P.J. Jansson, A. Arvind, P.C. Sharpe, M.T. Basha, G.M. Iskander, N. Kumar, Z. Kovacevic, D.J. Lane, S. Sahni, P.V. Bernhardt, D.R. Richardson, D.S. Kalinowski,

Novel mechanism of cytotoxicity for the selective selenosemicarbazone, 2-acetylpyridine 4,4-dimethyl-3-selenosemicarbazone (Ap44mSe): Lysosomal membrane permeabilization, J. Med. Chem. 59 (2016) 294-312.

[63] D. Hare, S. Ayton, A. Bush, P. Lei, A delicate balance: iron metabolism and diseases of the brain, Front. Aging Neurosci. 5 (2013) 34.

[64] T.B. Chaston, D.R. Richardson, Iron chelators for the treatment of iron overload disease: relationship between structure, redox activity, and toxicity, Am. J. Hematol. 73 (2003) 200-210.

[65] D.R. Crapper McLachlan, A.J. Dalton, T.P. Kruck, M.Y. Bell, W.L. Smith, W. Kalow, D.F. Andrews, Intramuscular desferrioxamine in patients with Alzheimer's disease, Lancet 337 (1991) 1304-1308.

[66] S. Mandel, T. Amit, O. Bar-Am, M.B. Youdim, Iron dysregulation in Alzheimer's disease: multimodal brain permeable iron chelating drugs, possessing neuroprotective-neurorescue and amyloid precursor protein-processing regulatory activities as therapeutic agents, Prog. Neurobiol. 82 (2007) 348-360.

[67] D.R. Richardson, K. Milnes, The potential of iron chelators of the pyridoxal isonicotinoyl hydrazone class as effective antiproliferative agents II: the mechanism of action of ligands derived from salicylaldehyde benzoyl hydrazone and 2-hydroxy-1-naphthylaldehyde benzoyl hydrazone, Blood 89 (1997) 3025-3038.

[68] D.R. Richardson, P. Ponka, The iron metabolism of the human neuroblastoma cell: lack of relationship between the efficacy of iron chelation and the inhibition of DNA synthesis, J. Lab. Clin. Med. 124 (1994) 660-671.

[69] D.S. Kalinowski, P.C. Sharpe, P.V. Bernhardt, D.R. Richardson, Structure-activity relationships of novel iron chelators for the treatment of iron overload disease: the methyl pyrazinylketone isonicotinoyl hydrazone series, J. Med. Chem. 51 (2008) 331-344.

[70] F.E. Harrison, R.J. Green, S.M. Dawes, J.M. May, Vitamin C distribution and retention in the mouse brain, Brain Res. 1348 (2010) 181-186.

[71] F.E. Harrison, J.M. May, Vitamin C function in the brain: vital role of the ascorbate transporter SVCT2, Free Radic. Biol. Med. 46 (2009) 719-730.

[72] A. Dutta, R. Gautam, S. Chatterjee, F. Ariese, S.K. Sikdar, S. Umapathy, Ascorbate protects neurons against oxidative stress: a Raman microspectroscopic study, ACS Chem. Neurosci. 6 (2015) 1794-1801.

[73] T.B. Chaston, D.B. Lovejoy, R.N. Watts, D.R. Richardson, Examination of the antiproliferative activity of iron chelators: multiple cellular targets and the different mechanism of action of triapine compared with desferrioxamine and the potent pyridoxal isonicotinoyl hydrazone analogue 311, Clin. Cancer Res. 9 (2003) 402-414.

[74] M. Shidore, J. Machhi, K. Shingala, P.M. Rumkar, M.K. Sharma, N. Agrawal, A. Tripathi, Z. Parikh, P. Pillai, M.R. Yadav, Benzylpiperidine-linked diarylthiazoles as potential anti-Alzheimer's agents: synthesis and biological evaluation, J. Med. Chem. 59 (2016) 5823-5846.

[75] A. Lleo, S.M. Greenberg, J.H. Growdon, Current pharmacotherapy for Alzheimer's disease, Annu. Rev. Med. 57 (2006) 513-533.

[76] M.B. Colovic, D.Z. Krstic, T.D. Lazarevic-Pasti, A.M. Bondzic, V.M. Vasic, Acetylcholinesterase inhibitors: pharmacology and toxicology, Curr. Neuropharmacol. 11 (2013) 315-335.

[77] M. Singh, M. Kaur, H. Kukreja, R. Chugh, O. Silakari, D. Singh, Acetylcholinesterase inhibitors as Alzheimer therapy: from nerve toxins to neuroprotection, Eur. J. Med. Chem. 70 (2013) 165-188.

[78] R.S. Keri, C. Quintanova, S.M. Marques, A.R. Esteves, S.M. Cardoso, M.A. Santos, Design, synthesis and neuroprotective evaluation of novel tacrine-benzothiazole hybrids as multi-targeted compounds against Alzheimer's disease, Bioorg. Med. Chem. 21 (2013) 4559-4569.

[79] R.A. Friesner, R.B. Murphy, M.P. Repasky, L.L. Frye, J.R. Greenwood, T.A. Halgren, P.C. Sanschagrin, D.T. Mainz, Extra precision glide: Docking and scoring incorporating a model of hydrophobic enclosure for protein-ligand complexes, J. Med. Chem. 49 (2006) 6177-6196.

[80] C.J. Maynard, A.I. Bush, C.L. Masters, R. Cappai, Q.X. Li, Metals and amyloid-beta in Alzheimer's disease, Int. J. Clin. Exp. Pathol. 86 (2005) 147-159.

[81] A.I. Bush, R.E. Tanzi, Therapeutics for Alzheimer's disease based on the metal hypothesis, Neurotherapeutics 5 (2008) 421-432.

[82] V. Albertini, L. Benussi, A. Paterlini, M. Glionna, A. Prestia, L. Bocchio-Chiavetto, G. Amicucci, S. Galluzzi, A. Adorni, C. Geroldi, G. Binetti, G.B. Frisoni, R. Ghidoni, Distinct cerebrospinal fluid amyloid-beta peptide signatures in cognitive decline associated with Alzheimer's disease and schizophrenia, Electrophoresis 33 (2012) 3738-3744.

[83] H. Schugar, D.E. Green, M.L. Bowen, L.E. Scott, T. Storr, K. Bohmerle, F. Thomas, D.D. Allen, P.R. Lockman, M. Merkel, K.H. Thompson, C. Orvig, Combating Alzheimer's disease with multifunctional molecules designed for metal passivation, Angew. Chem. Int. Ed. 46 (2007) 1716-1718.

[84] M.R. Jones, E.L. Service, J.R. Thompson, M.C.P. Wang, I.J. Kimsey, A.S. DeToma, A. Ramamoorthy, M.H. Lim, T. Storr, Dual-function triazole-pyridine derivatives as inhibitors of metal-induced amyloid-beta aggregation, Metallomics 4 (2012) 910-920.

[85] B.Y. Fang, D.J. Wang, M.F. Huang, G.H. Yu, H. Li, Hypothesis on the relationship between the change in intracellular pH and incidence of sporadic Alzheimer's disease or vascular dementia, Int. J. NeuroSci. 120 (2010) 591-595.

[86] M. Whitnall, J. Howard, P. Ponka, D.R. Richardson, A class of iron chelators with a wide spectrum of potent antitumor activity that overcomes resistance to chemotherapeutics, Proc. Natl. Acad. Sci. U.S.A. 103 (2006) 14901-14906.

[87] B. Ravikumar, S. Sarkar, J.E. Davies, M. Futter, M. Garcia-Arencibia, Z.W. Green-Thompson, M. Jimenez-Sanchez, V.I. Korolchuk, M. Lichtenberg, S. Luo, D.C. Massey, F.M. Menzies, K. Moreau, U. Narayanan, M. Renna, F.H. Siddiqi, B.R. Underwood, A.R. Winslow, D.C. Rubinsztein, Regulation of mammalian autophagy in physiology and pathophysiology, Physiol. Rev. 90 (2010) 1383-1435.

[88] D. Kliosnky, Guidelines for the use and interpretation of assays for monitoring autophagy, Autophagy 12 (2016) 443-443.

[89] S. Sahni, D.H. Bae, D.J. Lane, Z. Kovacevic, D.S. Kalinowski, P.J. Jansson, D.R. Richardson, The metastasis suppressor, N-myc downstream-regulated gene 1 (NDRG1), inhibits stress-induced autophagy in cancer cells, J. Biol. Chem. 289 (2014) 9692-9709.

[90] E. Gutierrez, D.R. Richardson, P.J. Jansson, The anticancer agent di-2-pyridylketone 4,4-dimethyl-3-thiosemicarbazone (Dp44mT) overcomes prosurvival autophagy by two mechanisms: persistent induction of autophagosome synthesis and impairment of lysosomal integrity, J. Biol. Chem. 289 (2014) 33568-33589.

[91] C.A. Lipinski, Lead- and drug-like compounds: the rule-of-five revolution, Drug Discov. Today Technol. 1 (2004) 337-341.

[92] D.E. Clark, Rapid calculation of polar molecular surface area and its application to the prediction of transport phenomena. 2. Prediction of blood-brain barrier penetration, J. Pharm. Sci. 88 (1999) 815-821.

[93] S.A. Hitchcock, L.D. Pennington, Structure-brain exposure relationships, J. Med. Chem. 49 (2006) 7559-7583.

[94] G.M. Sheldrick, A short history of SHELX, Acta Crystallogr. A 64 (2008) 112-122.

[95] L.J. Farrugia, WinGX suite for small-molecule single-crystal crystallography, J. Appl. Cryst. 32 (1999) 837-838.

[96] L.J. Farrugia, ORTEP-3 for Windows-a version of ORTEP-III with a Graphical User Interface (GUI), J. Appl. Crystallogr. 30 (1997) 565.

[97] D.R. Richardson, E. Baker, The uptake of iron and transferrin by the human malignant melanoma cell, Biochim. Biophys. Acta. 1053 (1990) 1-12.

[98] D. Richardson, E. Baker, Two mechanisms of iron uptake from transferrin by melanoma cells. The effect of desferrioxamine and ferric ammonium citrate, J. Biol. Chem. 267 (1992) 13972-13979.

[99] E. Baker, D. Richardson, S. Gross, P. Ponka, Evaluation of the iron chelation potential of hydrazones of pyridoxal, salicylaldehyde and 2-hydroxy-1-naphthylaldehyde using the hepatocyte in culture, Hepatology 15 (1992) 492-501.

[100] B.J. Iacopetta, E.H. Morgan, The kinetics of transferrin endocytosis and iron uptake from transferrin in rabbit reticulocytes, J. Biol. Chem. 258 (1983) 9108-9115.

[101] L. Pisani, R. Farina, M. Catto, R.M. Iacobazzi, O. Nicolotti, S. Cellamare, G.F. Mangiatordi, N. Denora, R. Soto-Otero, L. Siragusa, C.D. Altomare, A. Carotti, Exploring basic tail modifications of coumarin-based dual acetylcholinesterase-monoamine oxidase B inhibitors: identification of water-soluble, brain-permeant neuroprotective multitarget agents, J. Med. Chem. 59 (2016) 6791-6806.

[102] J. Sebestik, S.M. Marques, P.L. Fale, S. Santos, D.M. Arduino, S.M. Cardoso, C.R. Oliveira, M.L. Serralheiro, M.A. Santos, Bifunctional phenolic-choline conjugates as anti-oxidants and acetylcholinesterase inhibitors, J. Enzyme Inhib. Med. Chem. 26 (2011) 485-497.

[103] A. Nunes, S.M. Marques, C. Quintanova, D.F. Silva, S.M. Cardoso, S. Chaves, M.A. Santos, Multifunctional iron-chelators with protective roles against neurodegenerative diseases, Dalton Trans. 42 (2013) 6058-6073.

[104] G.L. Ellman, K.D. Courtney, V. Andres, Jr., R.M. Feather-Stone, A new and rapid colorimetric determination of acetylcholinesterase activity, Biochem. Pharmacol. 7 (1961) 88-95.

[105] M.P. Repasky, R.B. Murphy, J.L. Banks, J.R. Greenwood, I. Tubert-Brohman, S. Bhat, R.A. Friesner, Docking performance of the glide program as evaluated on the Astex and DUD datasets: a complete set of glide SP results and selected results for a new scoring function integrating WaterMap and glide, Journal of Computer-Aided Molecular Design 26 (2012) 787-799.

[106] J. Gao, D.R. Richardson, The potential of iron chelators of the pyridoxal isonicotinoyl hydrazone class as effective antiproliferative agents, IV: the mechanisms involved in inhibiting cell-cycle progression, Blood 98 (2001) 842-850.

Table 1. Anti-Proliferative Activity (IC_{50} in μM) of the Novel BPT Analogues and their Copper and Iron Complexes Against SK-N-MC Neuroepithelioma Cells, as Determined by the MTT Assay[a].

Compound	**Ligand (L)**	**Cu^{II}(L)**	**$Fe^{III}(L_2)$**
DFO	16.81 ± 3.87	9.83 ± 0.38	>25[b]
Dp44mT	0.013 ± 0.01	0.014 ± 0.01	2.00 ± 0.49
Donepezil	>100	83.33 ± 7.60	>100
PBPT	>100	46.18 ± 7.97	>100
SBPT	34.41 ± 1.24	1.30 ± 0.14	77.99 ± 11.58
NBPT	8.86 ± 0.10	1.81 ± 0.53	52.90 ± 8.34
PCBPT	4.23 ± 1.41	0.43 ± 0.02	1.33 ± 0.11
QBPT	17.71 ± 0.70	3.86 ± 1.28	1.20 ± 0.26
8-OH-QBPT	36.14 ± 3.24	1.87 ± 0.50	>100
2,3-OH-BBPT	16.85 ± 0.96	0.40 ± 0.09	23.99 ± 4.85
2,3,4-OH-BBPT	79.14 ± 0.36	12.22 ± 0.09	80.06 ± 13.57

[a]SK-N-MC cells (15,000 cells/well) were seeded in 96-well plates and incubated for 24 h/37°C and the cells then treated with control medium or compounds for 72 h/37°C. IC_{50} values are shown as mean ± SD (3 experiments).

[b]IC_{50} was measured for the 1:1 Fe^{III}-DFO complex (as dictated by stoichiometry).

Table 2. Calculated Physiochemical Properties of Tacrine, Donepezil and the BPT Analogues that Indicate Drug-Like Characteristics, including Blood-Brain Barrier (BBB) Permeation.

Compound	**M.W**[a]	**LogP**[a]	**HBA (N+O)**	**HBD (NH+OH)**	**Rot. bonds**[b]	**TPSA**[a]	**cLogP**[a]	**LogBB**[c]
Tacrine	198.27	2.91	2	2	0	38.38	3.27	0.07
Donepezil	379.50	4.01	4	0	6	38.77	4.60	0.26
PBPT	413.54	2.30	7	4	8	92.48	2.69	-0.82
SBPT	368.50	3.51	5	3	7	59.89	3.79	-0.17
NBPT	418.56	4.51	5	3	7	59.89	4.97	0.01
PCBPT	353.49	2.98	5	2	7	52.02	2.43	-0.26
QBPT	403.55	4.41	5	2	7	52.02	3.81	-0.05
8-OH-QBPT	419.55	4.02	6	3	7	72.25	3.91	-0.34
2,3-OH-BBPT	384.50	3.12	6	4	7	80.12	3.42	-0.53
2,3,4-OH-BBPT	400.50	2.73	7	5	7	100.35	2.82	-0.92
Required Parameters[d]	≤500	≤5	≤10	≤5	≤10	<90	2-5	>-1

[a]Calculated using ChemBioDraw Ultra14.0.

[b]Calculated using Cheminformatics (http://www.molinspiration.com/).

[c]LogBB = −0.0148 × TPSA + 0.152 × cLogP + 0.139.[92]

[d]Required parameters necessary to fulfill appropriate physiochemical properties as judged appropriate according to Lipinski's Rules and those important for BBB permeation [91-93].

Figures and Legends

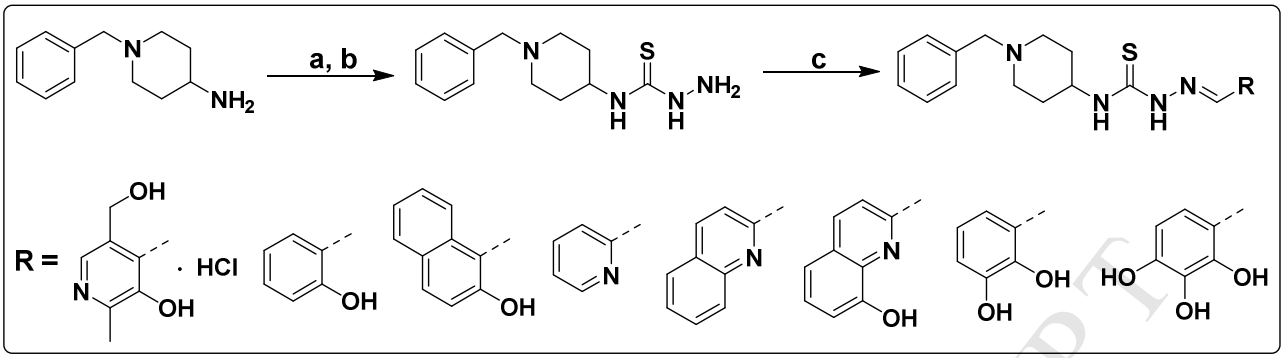

Scheme 1. Synthetic route for the preparation of the novel BPT series. Reagents and conditions: **(a)** CS_2, NaOH, H_2O, sodium chloroacetate, HCl, RT; **(b)** hydrazine hydrate, 90°C, 2 h; **(c)** aroyl aldehydes, ethanol, acetic acid, reflux, 2 h.

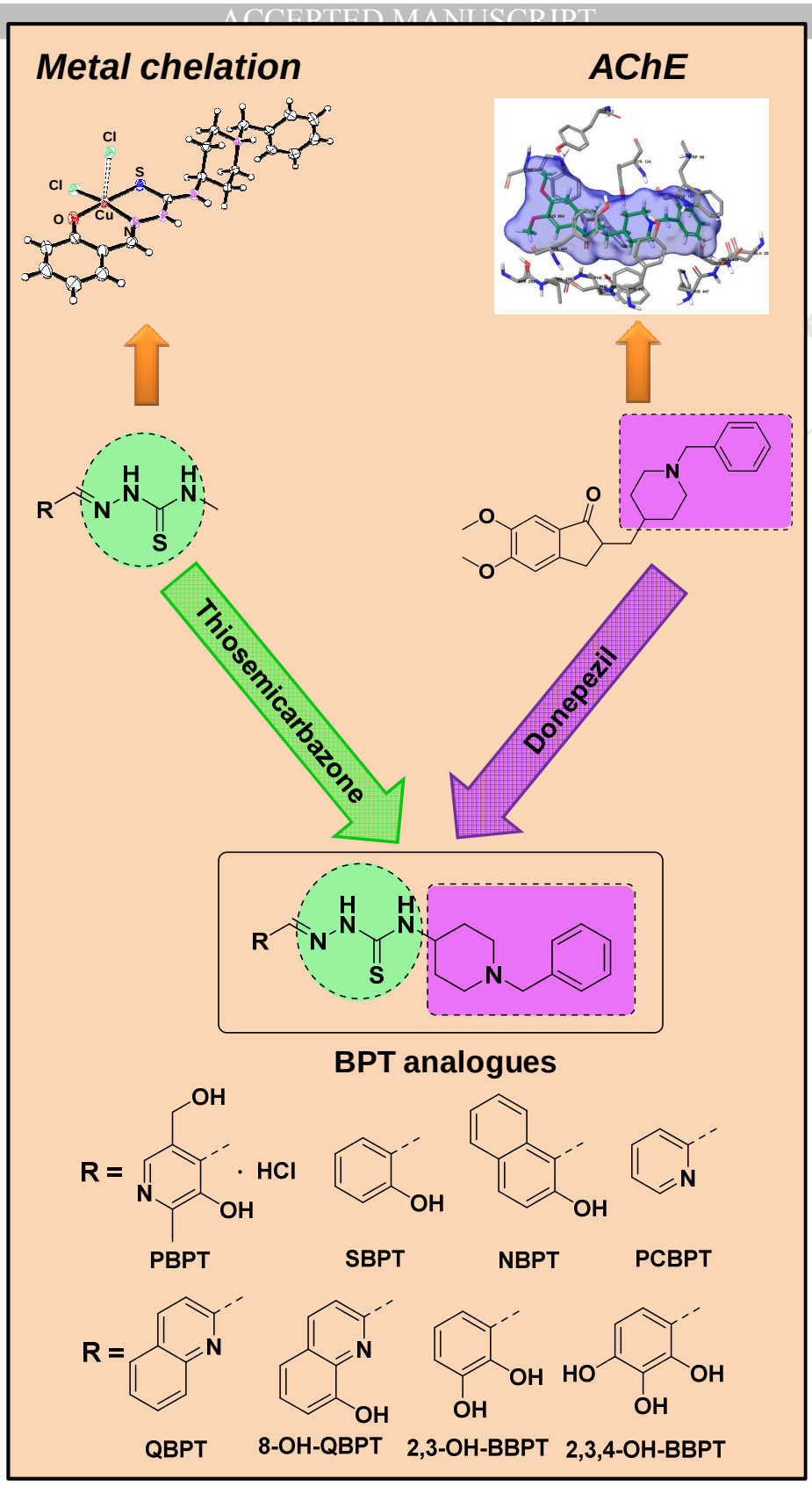

Figure 1. Design strategy utilized to generate the novel multi-functional 4-(1-benzylpiperidin-4-yl)thiosemicarbazone (BPT) series examined herein. This strategy combines pharmacophores from metal chelating thiosemicarbazones and the AChE inhibitor, Donepezil.

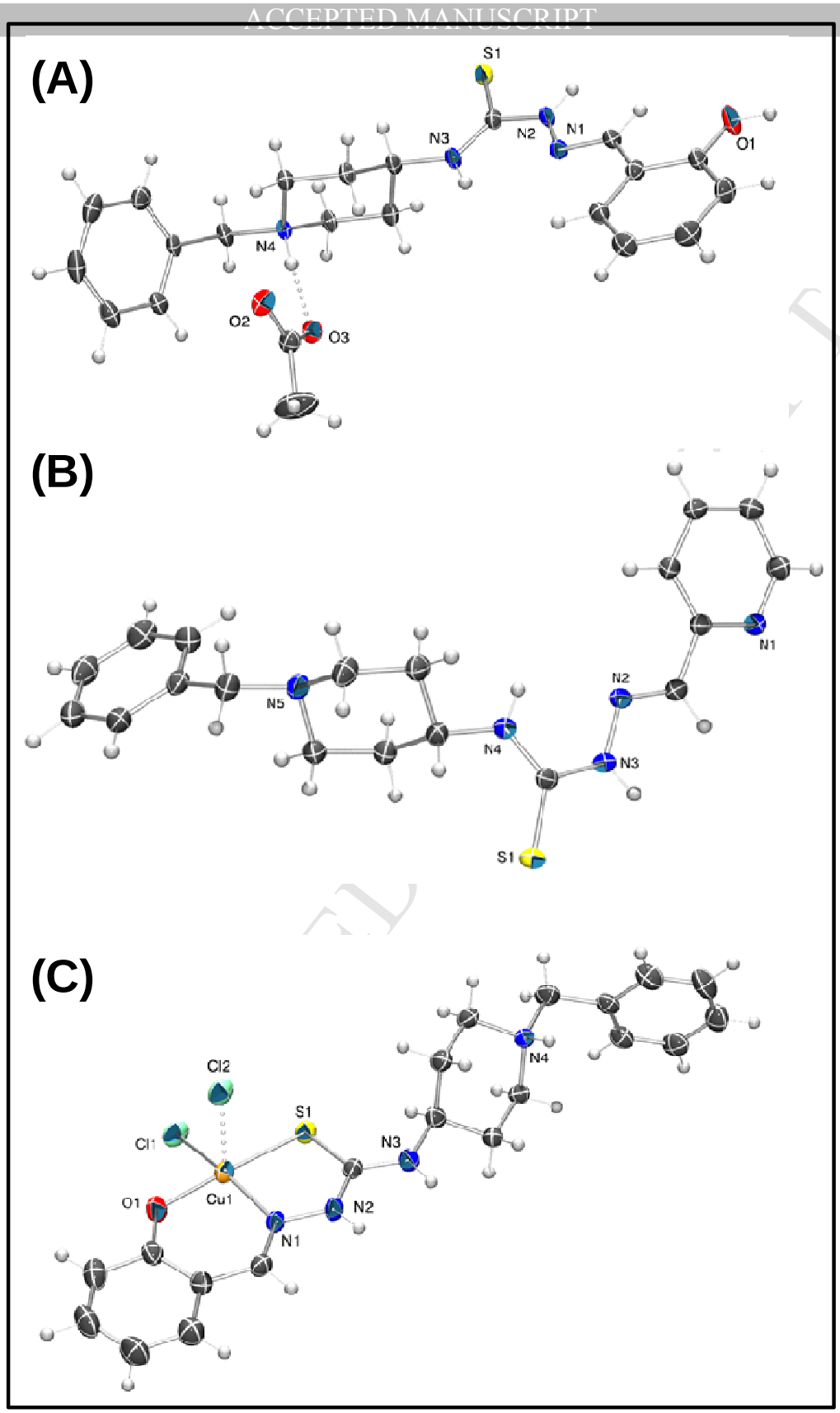

Figure 2. X-ray crystal structures of (A) [HSBPT][OAc], (B) PCBPT and (C) [Cu(SBPT)Cl_2].

Thermal ellipsoids were drawn at 50% probability level.

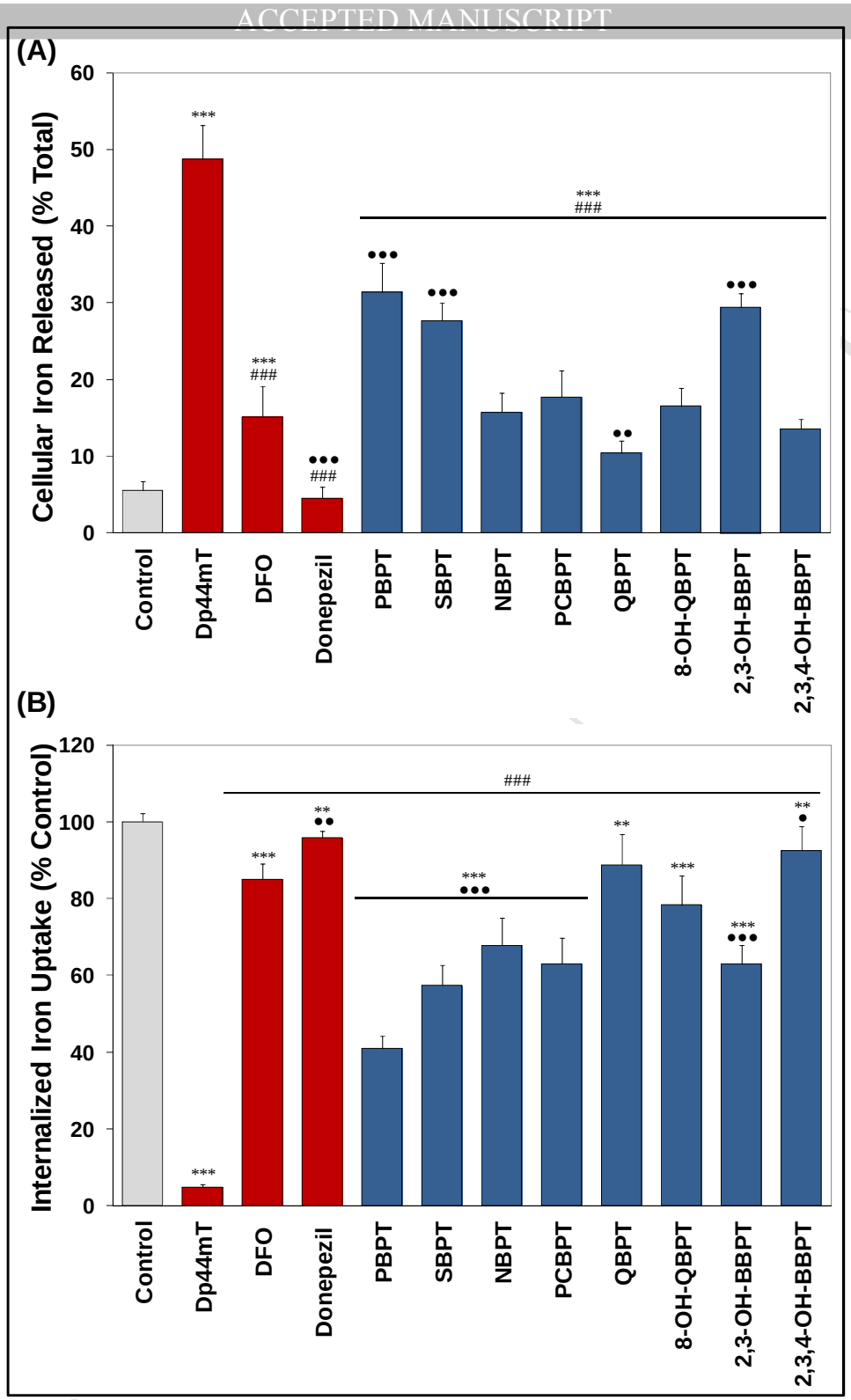

Figure 3. (A) The effect of the BPT series of analogues on ^{59}Fe release from prelabeled SK-N-MC neuroepithelioma cells. Cells were incubated with $^{59}Fe_2$-Tf (0.75 µM) for 3 h/37°C, washed four times with ice-cold PBS and then re-incubated in the presence or absence of the control compounds (25 µM) or novel BPT analogues (25 µM) for 3 h/37°C. The release of ^{59}Fe from the

cells mediated by the agents was then assessed. **(B) The effect of the BPT series of analogues on ^{59}Fe uptake from ^{59}Fe-transferrin ($^{59}Fe_2$-Tf) by SK-N-MC neuroepithelioma cells.** Cells were incubated with $^{59}Fe_2$-Tf (0.75 μM) alone (control), the control compounds (25 μM), or the novel BPT analogues (25 μM) for 3 h/37°C. The cells were then washed four times with ice-cold PBS, and incubated with protease (1 mg/mL) for 30 min/4°C to examine internalized ^{59}Fe uptake. Results are expressed as the mean ± SD (3 experiments). ** $p < 0.01$, *** $p < 0.001$ *versus* the control. $^{###}$ $p < 0.001$ *versus* Dp44mT. $^{•}p < 0.05$, $^{••}p < 0.01$, $^{•••}p < 0.001$ *versus* DFO.

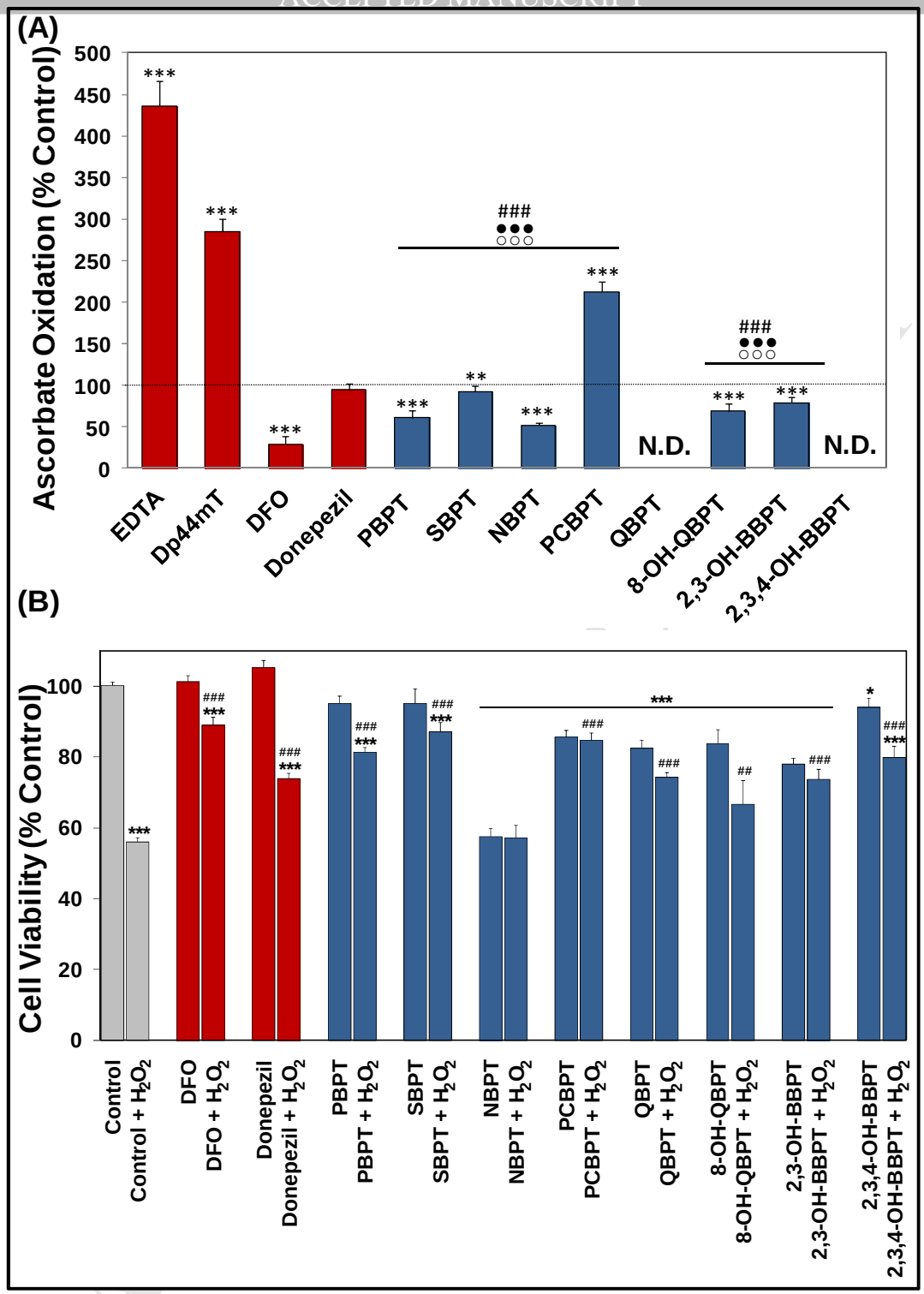

Figure 4. (A) The iron complexes of the novel BPT series of analogues do not lead to significant ascorbate oxidation. The assay was performed using an iron-binding equivalent (IBE) of 1. The Fe(III) complexes of EDTA, Dp44mT, DFO or Donepezil were used as controls. The activity of the control group containing $FeCl_3$ only was taken to be 100%. Results are mean ± SD (3 experiments). Activity of the Fe(III) complexes of QBPT and 2,3,4-OH-BBPT was not determined

(N.D.) due to their low solubility. $^{**}p < 0.01$, $^{***}p < 0.001$ *versus* the control. $^{\circ\circ\circ}p < 0.001$ *versus* EDTA. $^{\#\#\#}p < 0.001$ *versus* Dp44mT. $^{\bullet\bullet\bullet}p < 0.001$ *versus* DFO. **(B) The novel BPT series protect SK-N-MC neuroepithelioma cells against hydrogen peroxide-mediated cytotoxicity.** Cells were pre-incubated with the novel BPT series or the control compounds, DFO or Donepezil, at a concentration of 10 μM in serum-free medium for 2 h/37°C. The medium was removed and the cells were then incubated with fresh serum-free medium alone or serum-free medium containing H_2O_2 (150 μM) for 24 h/37°C. The cellular viability was measured using the MTT assay and the results are expressed as mean ± S.E.M. (3 experiments) as a percentage of the untreated control. $^{*}p < 0.05$, $^{***}p < 0.001$ *versus* the control. $^{\#\#}p < 0.01$, $^{\#\#\#}p < 0.001$ *versus* control cells incubated with H_2O_2.

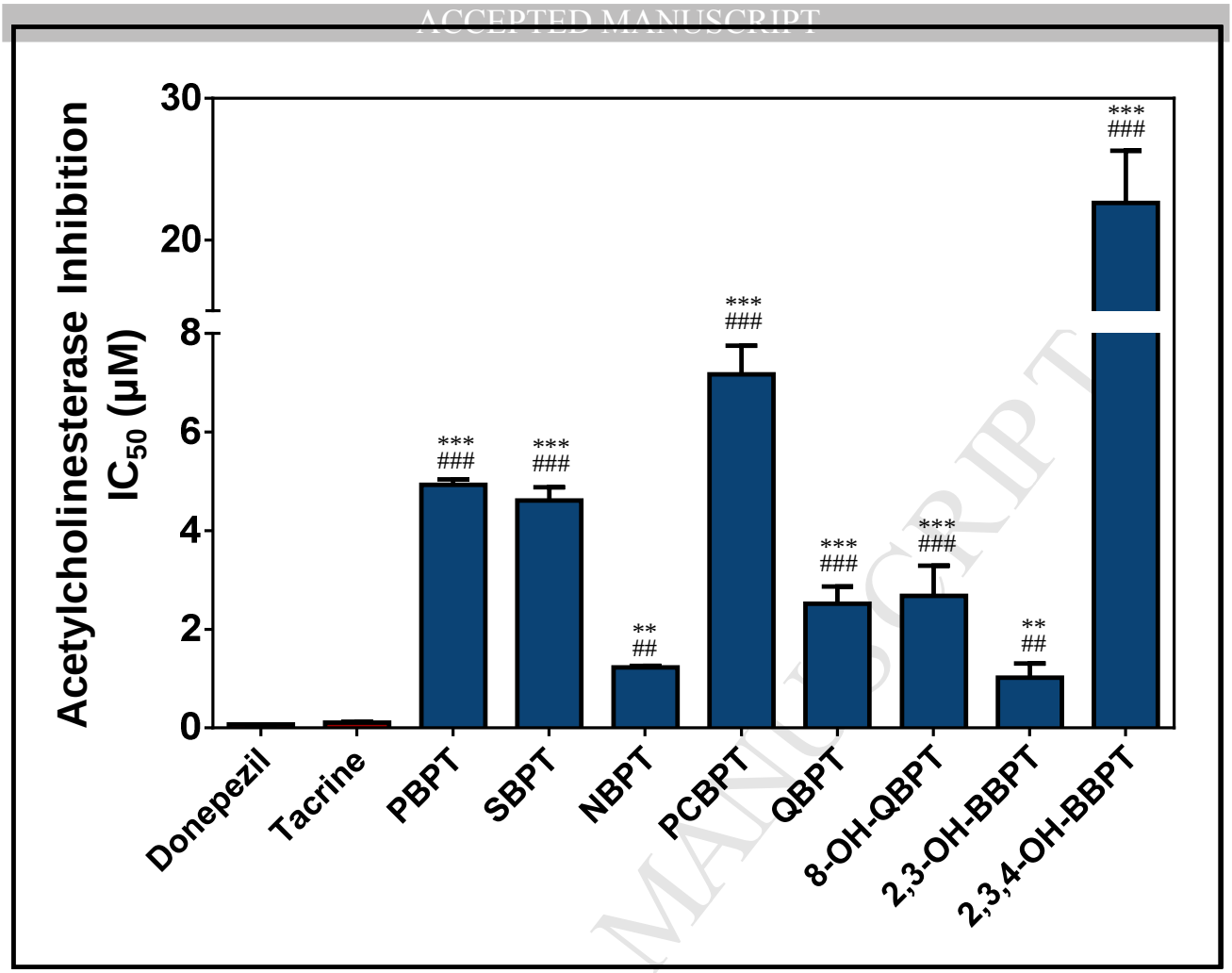

Figure 5. Several analogues of the BPT series show moderate inhibition of acetylcholinesterase (AChE) activity relative to the pronounced activity of the positive controls, Tacrine and Donepezil. In this assay, acetylthiocholine iodide is metabolized by AChE to form thiocholine and acetic acid. Thiocholine reacts with DTNB to form a yellow product, 5-thio-2-nitrobenzoic acid, whose formation was measured at 405 nm by UV-visible spectrophotometry. Results are mean ± SD (3 experiments). ** $p<0.01$ and *** $p<0.001$ *versus* Donepezil; $^{\#\#}$ $p<0.01$; $^{\#\#\#}$ $p<0.001$ *versus* Tacrine.

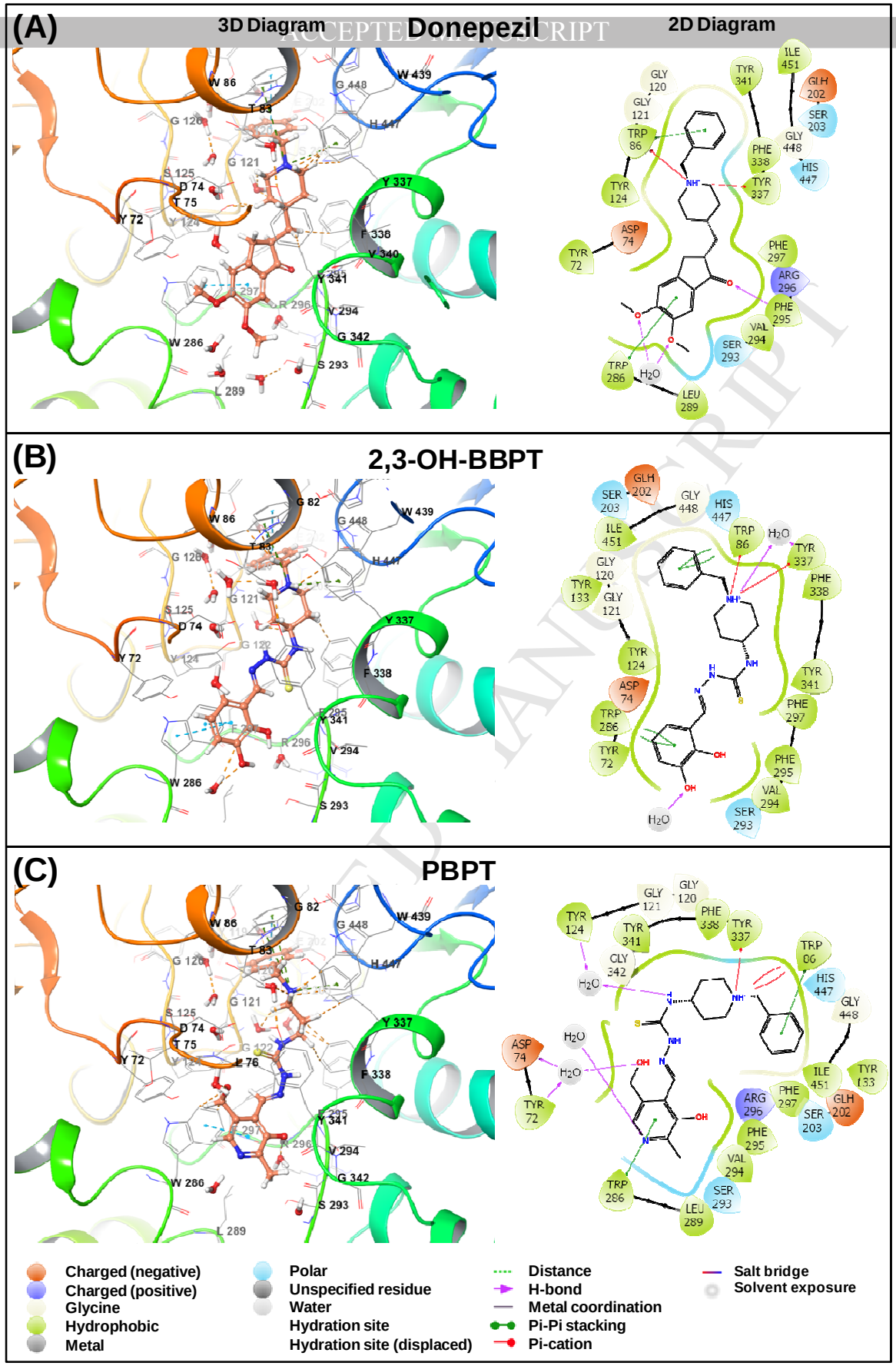

Figure 6. 3D and 2D docking diagrams showing the binding mode of (A) Donepezil, (B) 2,3-OH-BBPT and (C) PBPT in the active site of human AChE (PDB ID: 4EY7).

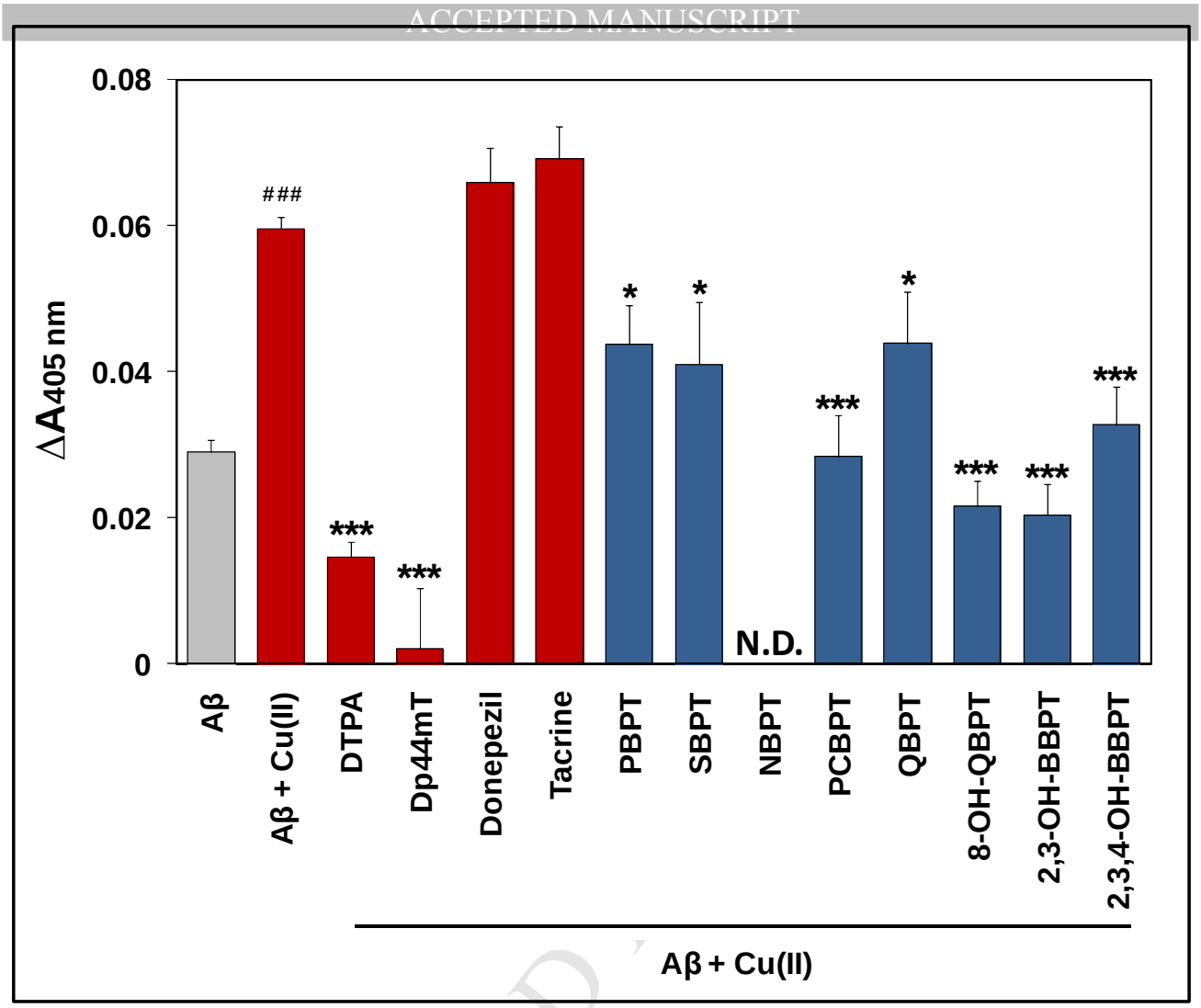

Figure 7. The effect of the BPT series of thiosemicarbazones on inhibiting the Cu(II)-mediated aggregation of $A\beta_{1-40}$. The aggregation of the $A\beta_{1-40}$ peptide was measured using an established turbidity assay at 405 nm after a 2 h incubation of $A\beta_{1-40}$ (25 μM) with Cu(II) (25 μM) in the presence or absence of the agents, including DTPA, Dp44mT, Donepezil, Tacrine and the BPT analogues (25 μM) in HEPES buffer (20 mM, 150 mM NaCl, pH 6.6). Results with NBPT could not be determined (N.D.) due to the low solubility of the compound. Results are presented as mean ± S.E.M. (3 independent experiments) using quadruplicates in each experiment. *$p < 0.05$, ***$p < 0.001$ *versus* Aβ + Cu(II); $^{###}p < 0.001$ *versus* Aβ.

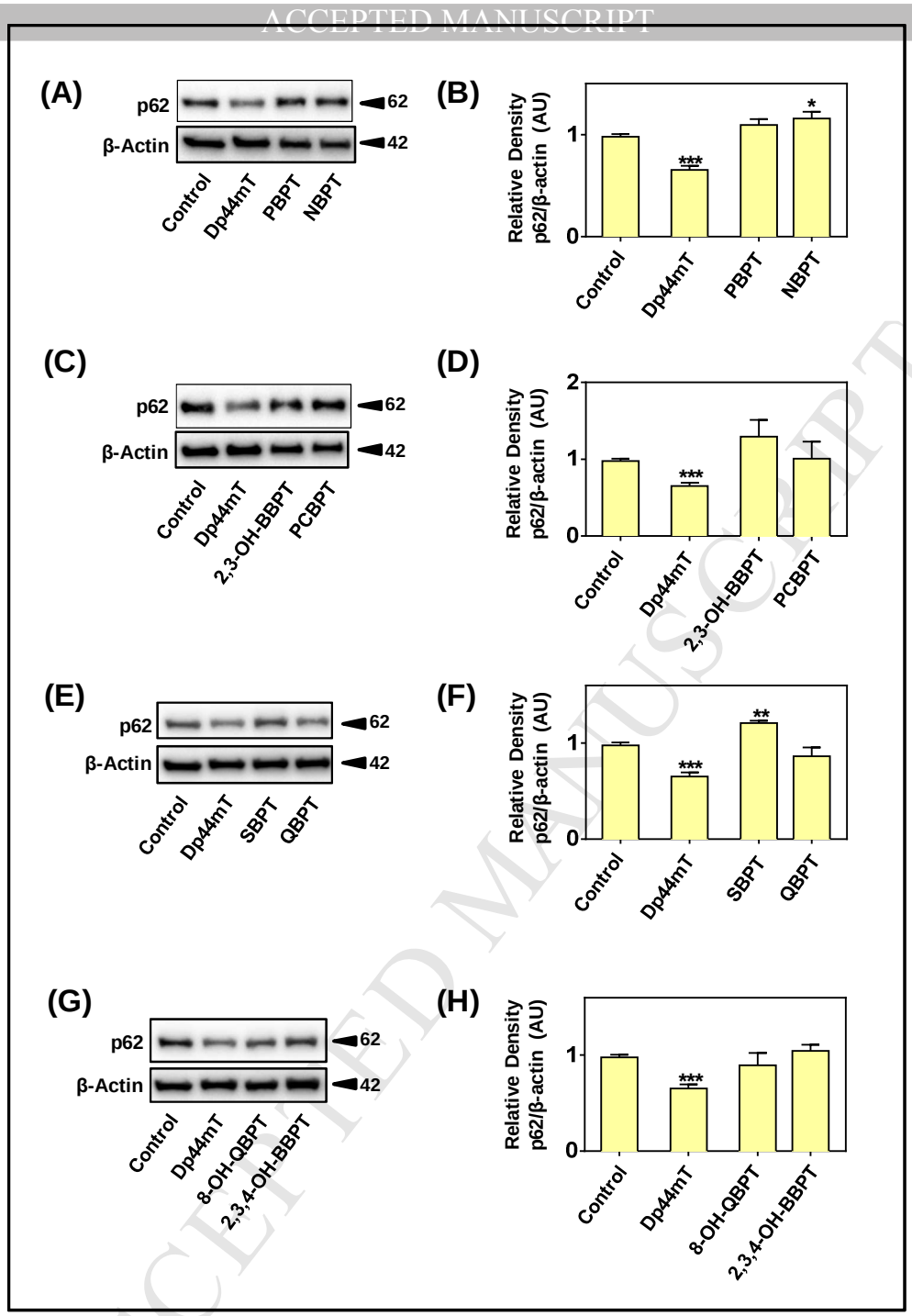

Figure 8. The effect of the BPT series of analogues on the levels of the autophagic marker p62 in SK-N-MC neuroepithelioma cells. (A, C, E, G) Western blots showing the effect of the BPT analogues (25 μM) on the levels of p62 that is a marker of autophagy after a 24 h incubation at 37°C. **(B, D, F, H)** Densitometry of p62 protein levels relative to the corresponding loading control (β-actin). Results are presented as mean ± SD (3 independent experiments). * p<0.05, ** p<0.01 and ***p<0.001 *versus* control.

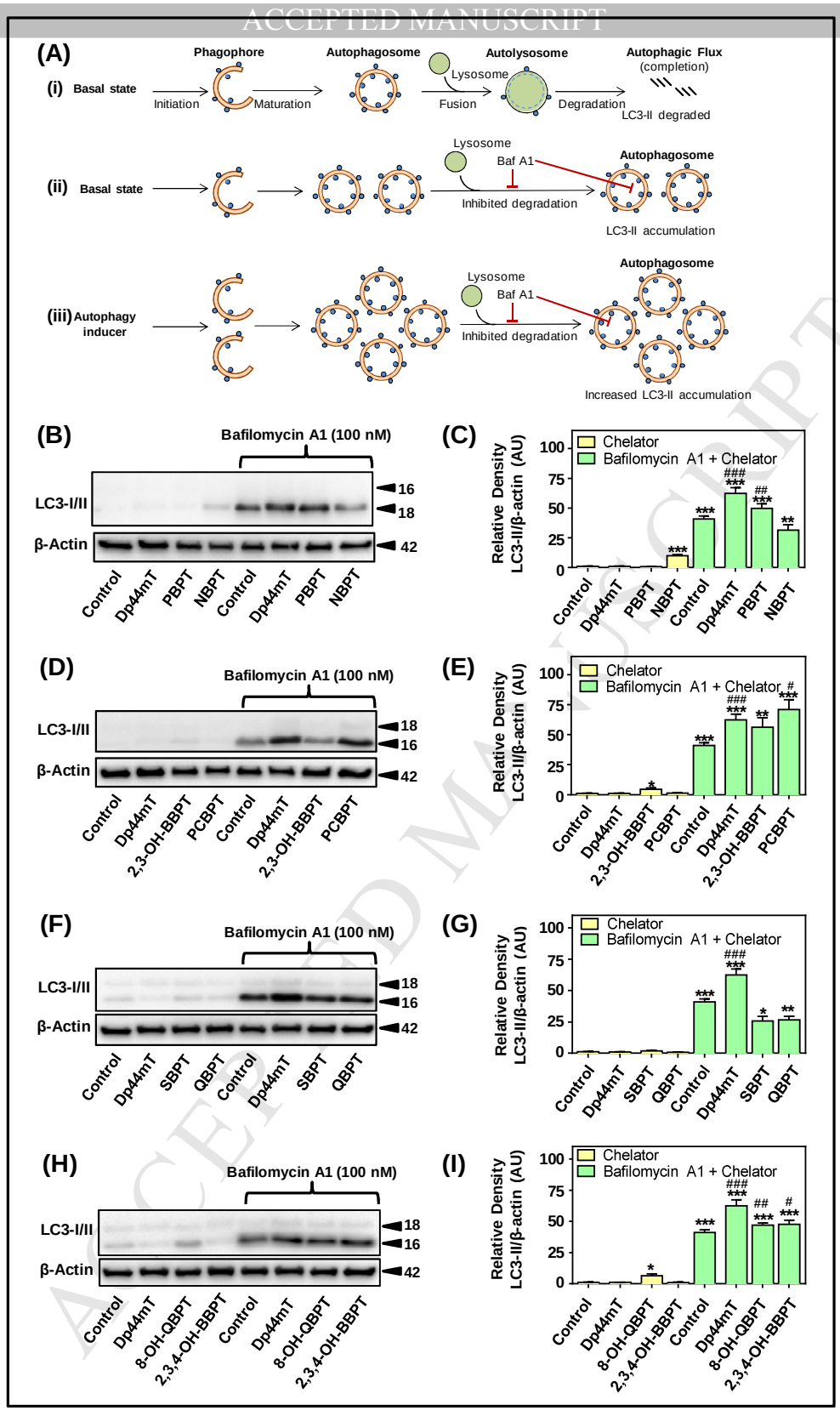

Figure 9. The BPT analogues, PBPT, PCBPT, 8-OH-QBPT, or 2,3,4-OH-BBPT, stimulate autophagic flux in SK-N-MC neuroepithelioma cells as measured using the autophagy inhibitor, Bafilomycin A1 (Baf A1). (A) Schematic diagram demonstrating the mechanisms by which total LC3-II protein levels (a classical marker of autophagosome formation) can be altered as

a consequence of changes in autophagosomal flux. **(i)** Under basal conditions, the newly formed autophagosomes are degraded upon fusion with the lysosome, leaving LC3-II levels unaltered. **(ii)** Autophagosome degradation is inhibited in the presence of Baf A1, which prevents autophagosome-lysosome fusion and leads to the accumulation of LC3-II. **(iii)** In the presence Baf A1, as well as an agent that induces autophagy (*e.g.*, Dp44mT), autophagosome formation is increased relative to basal levels and leads to further accumulation of LC3-II relative to Baf A1 alone. **(B, D, F, H)** Western blots showing the effect of the BPT analogues (25 μM) on the levels of LC3-II (18 kDa) after a 24 h incubation at 37°C in the presence or absence of the late-stage autophagy inhibitor, Baf A1 (100 nM). **(C, E, G, I)** Densitometry of LC3-II protein levels relative to the corresponding loading control (β-actin). Results are presented as mean ± SD (3 experiments). * $p<0.05$, ** $p<0.01$ and *** $p<0.001$ *versus* control. $^{\#}$ $p<0.05$, $^{\#\#}$ $p<0.01$ and $^{\#\#\#}$ $p<0.001$ *versus* the Baf A1 control.

Highlights

- New multi-functional thiosemicarbazones were designed for Alzheimer's disease (AD)
- The lead agent was pyridoxal 4-(*N*-(1-benzylpiperidin-4-yl)thiosemicarbazone (PBPT)
- PBPT showed substantial iron chelation efficacy and increased autophagic induction
- PBPT inhibited copper-mediated Aβ aggregation and acetylcholinesterase activity
- These properties show the potential of PBPT as a multi-functional AD therapeutic